공학박사 학위논문

Electronic and geometric structures of Pt / Au nanoparticles and their electrocatalytic activity

백금 / 금 나노 입자의 전자구조 및 기하하적 구조연구와 그에 따른 전기화학적 활성연구

2014년 2월

서울대학교 대학원

공과대학 화학생물공학부

정 동 영

Abstract

Electronic and geometric structures of Pt/Au nanoparticles and their electrocatalytic activity

Dong Young Chung

School of Chemical & Biological Engineering

Seoul National University

Due to being high efficient and environmentally friendly, proton exchange membrane fuel cells are one of the most promising next generation energy conversion devices to power the energy demands of the future. Substantial efforts are devoted to enhance the sluggish oxygen reduction reaction (ORR) at cathode compared to feasible hydrogen oxidation reaction at anode. The development of DFT-based theoretical understanding of the mechanisms of ORR yielded promising electrocatalyst materials. Pt is the most efficient ORR electrocatalyst due to the moderate intensity with adsorbate. To enhance the activity further, the oxygen species adsorption intensity should be lowered about 0.2 eV by DFT analysis. The Pt/Au structure was predicted that the lower activity owing to the lattice strain effects. The Au which atomic size is larger than Pt, induced the tensile strength and made the Pt d-band center up-shift with low degree of orbital overlap. High d-band center correlates to the high chemisorption energy and low ORR activity. Due to these expectations, few researches were conducted.

In this study, the Pt/Au nanoparticle systems were applied to the ORR electrocatalyst beyond the previous unfavorable expectation and single crystal

studies. The Au@Pt core-shell nanosized electrocatalysts and AuPt alloy nanoparticles were synthesized. Delicate investigations of nanoparticle structure were conducted using high resolution transmission electron microscopy and x-ray diffraction. X-ray absorption fine structures and photo emission spectroscopy also conducted at synchrotron facilities to confirm the inter-atomic distances, information related to the coordination numbers and electronic structures. From the CO stripping experiments, Pt-CO chemisorption energy was larger than that of the pure Pt until certain Pt surface compositions. However, the deposition of Pt increased, the Pt-CO chemisorption energy is lower than pure Pt which was controversy to previous predictions which the Au induced tensile strain to Pt with high chemisorption energy to CO and oxygen related species. To explain the experimental results, elucidations with quantum mechanics were performed. The chemisorption energy between metal and CO and oxygen species was interpreted two terms; center of d-band structures and orbital repulsion terms. The center of d-band positions was related to the band width. By changing the local environment, the d-band structure was changed due to the changing the orbital overlap between near atoms. Orbital repulsion terms were related to the adsorbate–metal orbital coupling matrix. The shorter the bond induced the more orbital overlap, the adsorbate anti-bonding orbital filled with the interaction between metal s,p orbitals. Due to the different electronegativity between Au and Pt, orbital repulsion should also be considered. Au has higher electronegativity compared to the Pt, induced the charge redistribution from Pt to Au. The lower electron in Pt induced the shorter bond distance with adsorbate, made the repulsion. The two parameters were mixed in Au/Pt systems. In the case of low Pt deposition to surface, the strain induced d-band center overwhelmed the effect of orbital repulsion terms. As amount of surface Pt increased, the strain factors decreased. Orbital repulsion factors were no longer the minor parameter at certain points. In the case of AuPt alloy nanoparticles, their flow

of electron redistribution was different to core-shell structures. Considering the electronic structures, the core-shell structures were good candidates for ORR electrocatalysts. The ORR activity trends also followed with the CO stripping results.

The different results between previous single crystal studies and current nanoparticle case were explained with the characteristics of nanoparticles. In the case of nanoparticles, their surface atoms have low coordinated which induces the surface atom contraction. Due to the surface contraction effect, the tensile strength was little effects on the Au@Pt system in nanoparticles. To confirm the nanosized atomic contraction effects, the surface coordination number was controlled using sonochemical method. The coordination number control was confirmed using extended x-ray absorption fine structures. The fitting parameter was shown as low coordination number, smaller inter-atomic distances and high Debye waller factors. Hydrogen oxidation reaction was also confirmed the surface low coordination number after sononchemical methods. After the coordination number controls, the Pt deposited to the Au nanoparticles. The lattice parameter of Pt was investigated using Rietveld refinement. The Pt deposited with low coordination numbered Au had low lattice parameter. Controlling the surface coordination number of core nanoparticle, strain could be controlled. The Au@Pt_0.5_S had 1.7 times higher ORR activity compared to without sononchemical method and 2.5 times higher activity compared to Pt nanoparticles.

From these researches, the possible factors related to the adsorbate chemisorption energy were considered; center of d-band structures and orbital repulsion under the quantum mechanics. The strain effects could be controlled with change of coordination number of nanoparticles. These considerations can be applied to the strategies to design the “nanoscale” electrocatalysts.

***Keywords*:** Electrochemistry, Electronic and geometric structure, Nanoparticle, Oxygen reduction reaction, Platinum / Gold

***Student Number*:** 2010-22821

Contents

List of Tables

List of Figures

Chapter 1. Introduction

1.1. Electrochemistry and Fuel cells

1.1.1. Electrochemistry kinetics

The electrochemical reaction is one of kinds of the chemical reactions, accompanied with electron transfer through the system. The electrochemical system composes of anode, cathode, electrolyte and external circuit. Involved in the system, electrons should be considered when to analyze the electrochemical reaction. Potential and current are commonly used as basic descriptors of the electrochemical reaction. An electrochemical potential is defined as the sum of the chemical and the electric potential. Therefore, the equilibrium potential can be formulated by the equation, so-called Nernst equation;

$$E_{eq} = E^0 + \frac{nF}{RT}\left(\sum_i \ln a_i^o - \sum_j \ln a_j^R\right)$$

where, E_{eq}, E^o, n,F, R, a^O, and a^R are equilibrium potential, standard potential, number of electrons, Faradaic constant, ideal gas constant, activity of oxidants, and activity of reductants, respectively.

Current can be expressed by the sum of the rate of reaction of the anode and the cathode. The equation shows the correlation of the current and the kinetic of reaction.

$$i_{net} = i_0 \left[\frac{C_O(0,t)}{C_O^*} e^{-\frac{\beta nF(E-E_{eq})}{RT}} - \frac{C_R(0,t)}{C_R^*} e^{\frac{(1-\beta)nF(E-E_{eq})}{RT}} \right]$$

where, i_0, β, E, E_{eq}, C_O^*, C_O, C_R^*, and C_R are exchange current, symmetry factor, applied potential, equilibrium potential, bulk concentration, concentration of oxidant, and those of reductants, respectively.

Electrochemical cells are classified into two types, a galvanic cell and an electrolytic cell. The galvanic cell is an electrochemical cell that derive energy from the spontaneous reaction such as fuel cell and. In the galvanic cell, the overpotential, difference in reduction potential between the thermodynamic and the measured value, has a negative effect on the total cell efficiency. To improve the cell efficiency, it is important to minimize the overpotential in the electrode where the electrochemical reaction takes place. The other is

1.1.2. Proton Exchange Membrane Fuel Cell (PEMFC)

A fuel cell is an energy conversion device, generating electricity from electrochemical reaction with oxygen and hydrogen.[1] The anode reaction is hydrogen oxidation reaction (HOR) which is feasible reactions compared to cathode reaction. However the oxygen reduction reaction (ORR) in cathode is extremely sluggish reaction. The overpotential for ORR reaction is about 10 times larger than HOR reaction. The state of art electrocatalyst for both anode and cathode is platinum. The cathode catalyst such as Pt group metal is extremely expensive and rare. Due to the cost issues, reducing the noble metal by core-shell and alloying has been suggested. However, the enhancement was not satisfied to commercialize the fuel cells. The second problem is durability issues. The PEMFC operation environments are extremely harsh condition. High temperature (above 70 ^{o}C), acidic and oxidizing condition affects the material stability. Especially, the nanoscale electrocatalyst, which is concerned for real application based on the superiority for mass activity, agglomerated and dissolved during operation. To enhance the durability, several solutions have been reported. Changing the support materials such as oxide and CNT can enhance the durability. Strong metal support interaction between metal oxide and carbon prevent dissolution and agglomeration. Hollow and nanowire structure has been reported with high durability. Specific facets with low surface energy such as (111) correlated to the superior durability. Modified with Au is another method to enhance the stability dramatically. Zhang et al. reported that the Au modified Pt can be durable up to 30,000 cycles.[2] Finally, CO poisoning and impurity are critical

issues.[3] The small amount of CO can poison the Pt, deactivate the catalyst significantly. Although some strategies exhibit enhanced tolerance of CO, Pt still remains a limiting factor in the overall performances.

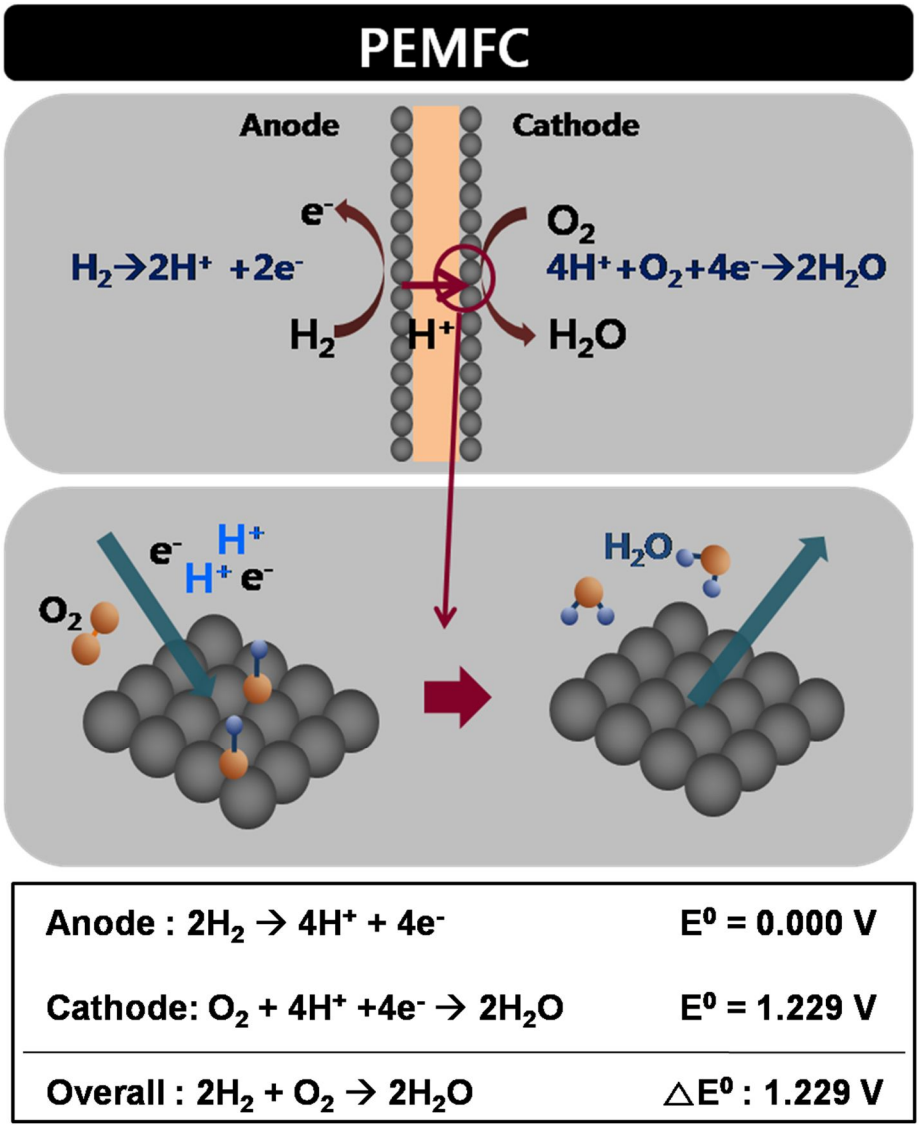

Anode : $2H_2 \rightarrow 4H^+ + 4e^-$	$E^0 = 0.000$ V
Cathode: $O_2 + 4H^+ + 4e^- \rightarrow 2H_2O$	$E^0 = 1.229$ V
Overall : $2H_2 + O_2 \rightarrow 2H_2O$	$\triangle E^0 : 1.229$ V

Figure 1.1. Electrochemical reactions in the PEMFC.

1.2. Oxygen reduction reaction

1.2.1. Oxygen Reduction Reaction (ORR)

The cathode reaction in PEMFC is the oxygen reduction reaction. The ORR is four electron reactions which may include the numbers of elementary reactions involving electrochemical and chemical reactions. The exact ORR mechanisms are still under debate. However, in the case of the Pt group metal, the associate mechanisms are dominant at the operation conditions which the oxygen coverage is large at high potentials.[4] The reaction rate of ORR could be described as follows:

$$i = nAFk^0 C_{O_2}(1-\theta_{ad}) \exp\left(-\frac{\gamma r \theta_{ad}}{RT}\right) \exp\left(-\frac{\alpha F \eta}{RT}\right)$$

where, n is the electron transfer number, A is the geometric area, k_0 is the rate constant, C_{O2} is oxygen concentration in electrolyte, θad is the coverage of adsorbate to catalyst surface and β and γ is the transfer coefficient (assumed to be 0.5). The symmetry factor, α is the transfer coefficient which describes the symmetry of the barrier. r is the interaction parameter describing the rate of change of standard Gibbs free energy of adsorption with the surface coverage of adsorbing ions, and η is the overpotential.

The kinetic current j_k can be obtained equations as follows:

$$\frac{1}{j} = \frac{i}{j_L} + \frac{1}{j_k}$$

This empirical equation can be explained using absolute rate theory. Assuming a linear dependence of the activation Gibbs energy, ΔG^*. The kinetic current density for oxygen reduction is given by the Butler-Volmer equation

$$j_k = -j_0 \left[\exp(-\beta n f \eta) - \exp\left((1-\beta) n f \eta\right)\right]$$

Platinum has the highest activity among the single metals, but is still room for improvement of its electrochemical reactivity.[4] Considering the mechanisms, the overpotential of ORR for Pt is originated from too strongly adsorption of oxygen species to the catalyst surface. In order to decrease overpotential of ORR, it is favorable that the strength of chemisorbed species is slightly weakened.

By taking into consideration of the adsorption energy of oxygen species, overall free energy for the reaction can be calculated. From the potential dependent free energy diagrams, the major thermodynamic uphill is fourth electron transfer step in the case of Pt.[4] To low the activation energy of fourth step, the chemisorption energy between Pt to oxygen species can be lowered. For metals that bind oxygen too strongly, the rate is limited by the removal adsorbate.[5] For metal surfaces that bind the oxygen too weakly, the rate is limited by the dissociation of oxygen or adsorption of oxygen. However the lowest chemisorption energy cannot relate to the highest activity.

As the chemisorption energy decrease, the first electron transfer step can be thermodynamically uphill. Due to the complex and inter related with the oxygen species in ORR steps, the moderate chemisorption energy should be important.[6] The ‘moderate’ chemisorption energy means the highest ORR activity can be possible at certain points. In the case of the high chemisorption energy compared to the optimal chemisorption energy, the activity decrease due to the fourth electron transfer step has high overpotential. However in the case of low chemisorption energy, the activity also decreased due to the first step. This volcano like activity trends was well matched with classical Sabatier’s principles.[4][7]

To achieve this goal, we need to tailor the Pt electronic structure, the frontier d-band structure directly associated with the extent of chemisorption and the activation barrier. The electronic structure of Pt can be altered by changes in the surface structure with the different facets and the ligand effect including alloying.[8-11]One of the most common approaches is alloying with other metallic species and core-shell structures. This effect also causes the shift of the frontier d-band structure of Pt by calculations and experimental results.[12]

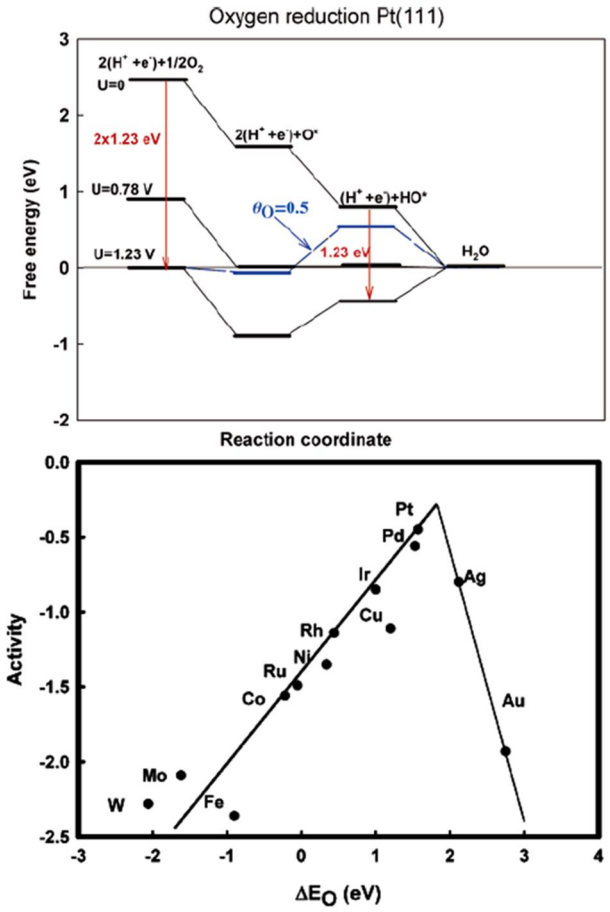

Figure 1.2.ORR mechanisms at different potentials and surface oxygen compositions. Volcano plots of the oxygen chemisorption energy and oxygen reduction activity (Adapted from the J.K. Norskov et al., J. Phys. Chem. B, 2004, 108,17886)

1.2.2. Electronic and geometric structures and related to the ORR activity.

When an adsorbate species is approached to d-group metals, it is known that s-bands widen their width due to the strong coupling with the valance states of adsorbates. The d-band width is narrow due to the small coupling matrix which is proportional to the band width. Considering the simple one electron model which concerns atoms and molecules interacting with a metal surface, the valance states of adsorbate species separate the states into a bonding and an anti-bonding state. A bonding state has a lower energy level with respect to Fermi level of metals. An anti-bonding state shows resistive characters to adsorption on the metal surface with an unstable energy state.

The degree of split-off bonding and anti-bonding states is related to the chemisorption energy. The strong chemisorption induce separation of two states in adsorbate species as well as the shift up of d-band center in metal species to the Fermi level due to decrease in width of d-band. Therefore, the center of d-band is a fine descriptor which can estimate the strength of chemisorption energy between a metal and an adsorbate.[13]

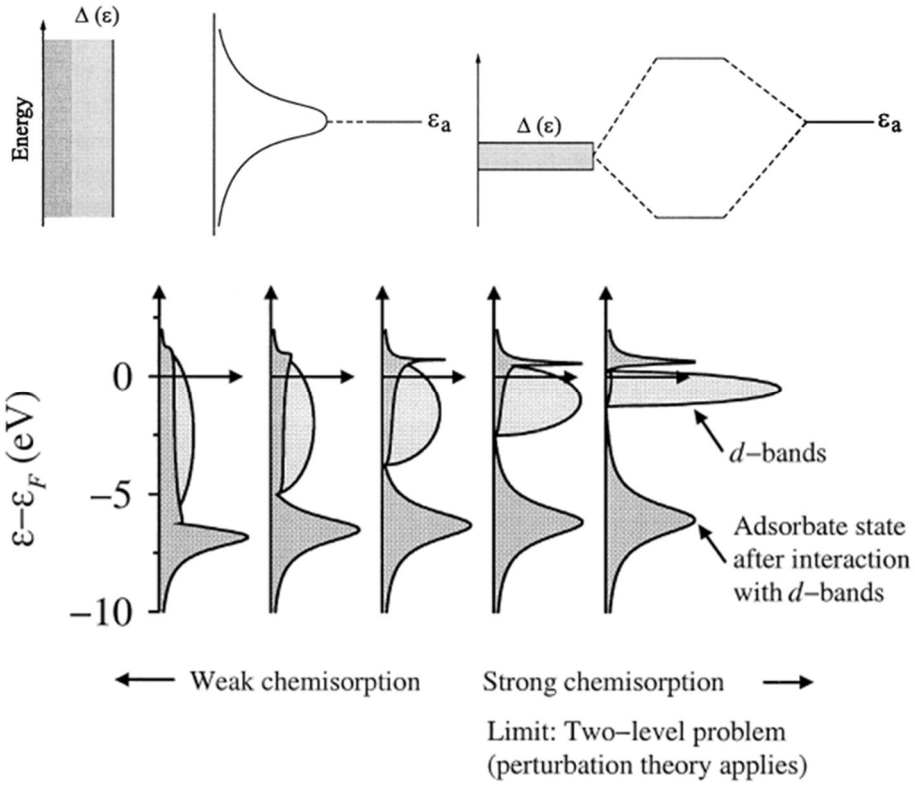

Figure 1.3. Density of states for adsorbate state interacted with the different orbitals (Adapted from the B. Hammer and J.K. Norskov et al., Adv. Catal., **2000**, 45,71)

Nørskov et al., suggested that the adsorption energy is linear correlation with the activation energy of reaction intermediates independent of reactant species[14], so-called Brønsted–Evans–Polanyi lines.[15] Like the adsorption strength of adsorbate species, it can be characterized by the center of d-band. In summary, tuning the electrocatalyst, three possible factors are affected to the activity; ensemble effects[16, 17], ligand effects[18-22] and geometric effects.[20, 22-25] Ensemble effects mean that dissimilar surface atoms take on distinct mechanistic functionalities. Ligand effect is related to the electronic charge redistribution. The geometric effect is related to the atomic rearrangement of surface atoms and strain effects. In the case of compressive strains, the atomic orbital between metal increased. The increased atomic orbital induce the d-band width change. In the case of compressive strain, the band widths are broad. However the Fermi level of metal does not change during local environment change. The Fermi level is thermodynamic values.

The core-shell structure is promising solutions to enhance the electrocatalytic activity. Unlikely homogenously alloyed particles, core-shell particles offer a large variety of structural and compositional parameters, such as shell thickness, compositions of core, core size and particle shape.[26] Understanding of their effects on activity and stability by

tailoring the critical parameters is the main key for the design of efficient and robust catalysts. Recently, many approaches related to the core-shell have been suggested.[25, 27-37]

1.2.3 Research trends of Au/Pt systems for oxygen reduction reaction

The research on the Au/Pt systems for oxygen reduction reaction was not fully conducted due to the theoretical unfavorable expectation. J. Zhang et al. reported that unprecedented high durability by simply modifying the Pt/C catalyst with Au.[2]Gold cluster deposited Pt catalyst can be stabilized against dissolution under potential cycling. From the in-situ x-ray absorption near-edgy spectroscopy, Au modified Pt has less oxidized under potential increase. The exact reason for the enhancing the durability, Au can be the potential materials for high stability. After then many researches of Au/Pt high durable electrocatalyst were suggested.[38-40] However, the ORR activity was below the Pt or slightly enhanced. The detail view of Au/Pt systems for ORR was not conducted. Recently, Our groups reported that the importance of surface Pt composition in AuPt alloy system for ORR activity by segregation of Pt at CO environment.[41] As the surface composition of Pt increased, the specific activity increased. However, the reasons of activity enhancement were not fully understand. The activity trends of AuPt were not identical.[39, 40, 42-53] The difference trend compared to Pt may be related to the thermodynamic issues. The surface free energy of Au is lower than that of the Pt. However, the standard reduction potential of Au is higher than that of the Pt. The homogeneous

AuPt alloy is favored only the size is below the 5 nm. Because the exact surface composition and structure was not confirmed, the activity trends may be complex. Delicate structure analysis and electrocatalytic activity studies should be required.

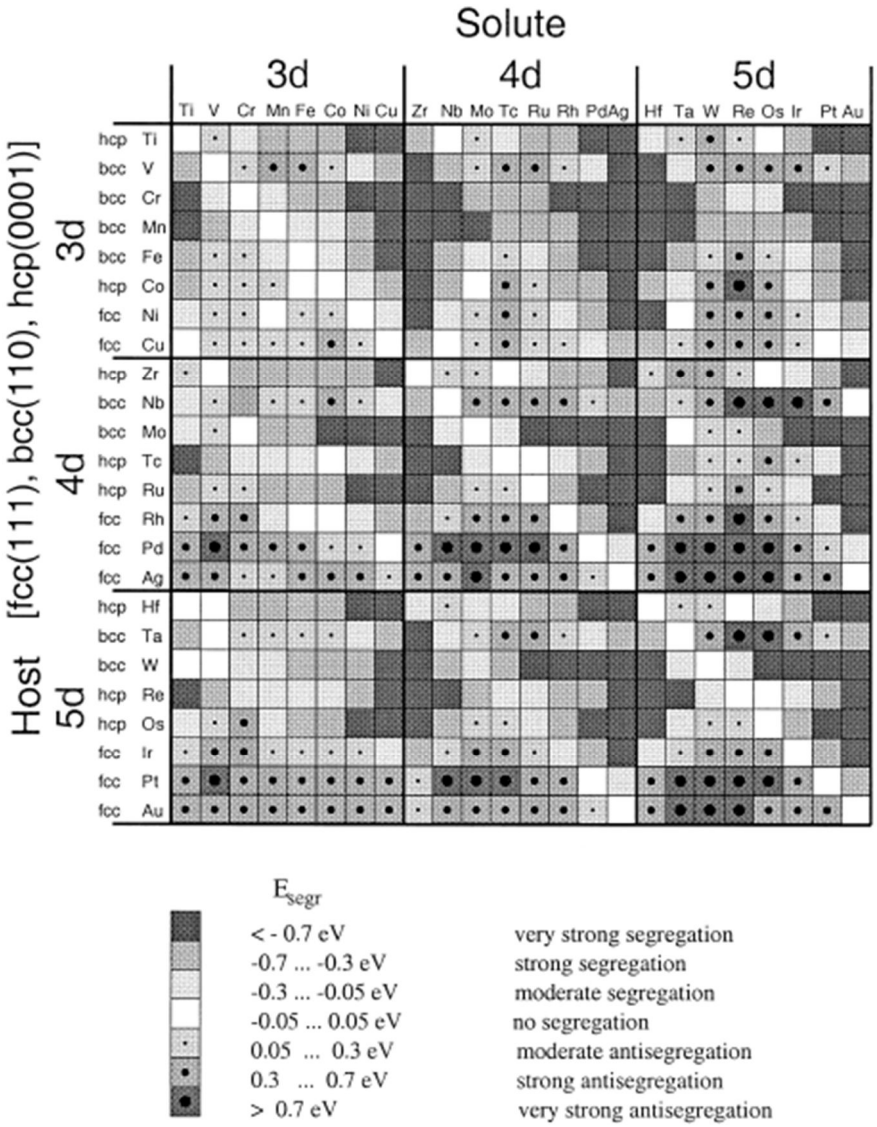

Figure 1.4. Compilation of calculated segregation energies on the most close-packed surface of all binary combination of transition metals. (Adapted from the Christensen et al.,Phys. Rev. B, **1999**, 59,15900)

1.3. Objectives of this dissertation

In this study, the Pt/Au nanoparticle systems were applied to the ORR electrocatalyst beyond the previous unfavorable expectation and single crystal studies. Delicate investigations of nanoparticle structure were conducted using synchrotron based techniques and state of art physical characterizations.

The discrepancy between theoretical explanation and current research was explained based on the quantum mechanics. The chemisorption energy between metal and adsorbate was interpreted two terms; center of d-band structures and orbital repulsion terms. By changing the local environment, the d-band structure was changed due to the changing the orbital overlap between near atoms. Orbital repulsion terms were related to the adsorbate–metal orbital coupling matrix. The shorter the bond induced the more orbital overlap, the adsorbate anti-bonding orbital filled with the interaction between metal sp orbitals. In previous, the orbital repulsion term was not considered in the screening the electrocatalyst for ORR. However, second parameter should be considered when the electronegativity difference exists such as Au@Pt cases.

The different results between previous single crystal studies and current nanoparticle case were explained with the characteristics of nanoparticles.

In the case of nanoparticles, their surface atoms have low coordinated which induces the surface atom contraction. Due to the surface contraction effect, the tensile strength was little effects on the Au@Pt system in nanoparticles. The importance of electronic and geometric structure analysis was considered by reflection of special Au/Pt system. From the basic concerns, the parameter could be further controlled in nanoscale systems.

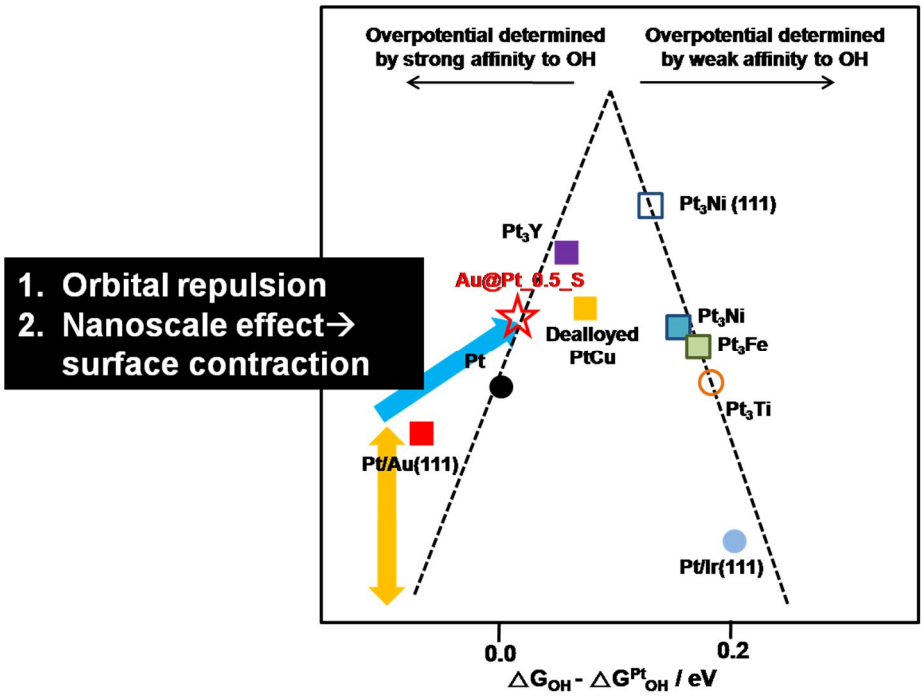

Figure 1.5. Subjects of this thesis.

Chapter 2.Experimental

2.1. Preparation Stage:

2.1.1. Chemicals and Materials

Vulcan XC 72-R (Cabot Corp., Boston, MA, USA), $HClO_4$ (Aldrich, ACS reagents), $NaBH_4$ (Sigma Aldrich, ACS reagent), $HAuCl_4 \cdot 3H_2O$ (Sigma Aldrich, ACS reagent), $H_2PtCl_6 \cdot xH_2O$ (Sigma Aldrich, ACS reagent), $PtCl_4$ (Sigma Aldrich, ACS reagent), Sodium citrate (Sigma Aldrich, ACS reagent), H_2SO_4 (Sigma Aldrich, ACS reagent), All aqueous solutions were used with deionized (DI) water, which was purified using Milli-Q system (18.2 MΩ cm; millipore, Bedford, MA, USA)

2.1.2. Synthesis of AuPt(alloy) nanoparticles

Carbon supported AuPt alloy nanoparticles were synthesized via conventional sodium borohydride reduction in aqueous solution at room temperature. All chemicals were purchased from Sigma Aldrich and used without further purification. To a beaker (1000 ml), appropriate amount of chloroplatinic acid ($H_2PtCl_6 \cdot xH_2O$), chloroauric acid ($HAuCl_4 \cdot 3H_2O$) and citrate ($Na_3C_6H_5O_7$, 0.1 g) was dissolved in 800 ml of DI water. Under

vigorous stirring, sodium borohydride ($NaBH_4$, 0.03 g) and sodium citrate ($Na_3C_6H_5O_7$, 0.1 g) were added. After thirty minutes, 0.075 g of carbon (Vulcan XC-72R) was added to the solution and stirred 24 hr and followed by addition of 200 ml of a 0.1 M $HClO_4$ solution and then filtered.

2.1.3. Synthesis of Au@Pt(core-shell) nanoparticles

Synthesis of Au nanoparticles.

Carbon supported Au nanoparticles were synthesized modified borohydride method.[54-56] Au colloid nanoparticles were prepared by stirring Au precursor ($HAuCl_4$ $3H_2O$, 0.0579 g) into 800 ml of H_2O. This was followed by the addition of sodium citrate ($Na_3C_6H_5O_7$, 0.1 g) after 1 min. After additional 1 min, sodium borohydride ($NaBH_4$, 0.03 g) and sodium citrate ($Na_3C_6H_5O_7$, 0.1 g) were added under vigorous stirring.

Synthesis of Au@Pt_x nanoparticles.

Pt deposition on the surface of the metal nanoparticles follows the same procedure as previous reports.[57, 58] An appropriate amount of Au/C (30wt. %) was dispersed in anhydrous ethanol and sonicated 10min. Platinum (IV) chloride and hydroquinone (HQ) was dissolved in anhydrous ethanol. (molar ratio of HQ : $PtCl_4$ = 20 :1) This solution was stirred under

Ar condition to remove the oxygen sources. The solution was heated to 70 ^{o}C and kept for 2 h at this temperature. The solution was cooled at room temperature and filtered.

2.1.4. Physical characterization

Conventional normal transmission electron microscopy (TEM) was measured using JEM-2100 (200 kV, JEOL) and high resolution transmission electron microscopy (HR-TEM) was measured using Tecnai F20 (200 kV, FEI). Aberration-corrected high resolution transmission electron microscopy (Aberration-corrected HR-TEM) was measured using JEOL JEM-2200FS (with Image Cs corrector) at National Institute of Nanomaterials Technology (NINT) and JEM-ARM200F (with STEM Cs corrector, EDS, BrukerQuantax 400) at National NanoFab Center (NNFC)

X-ray diffraction (XRD, Rigaku D/MAX 2500) spectra were obtained with Cu Kα(0.1541 nm) at 40 kV and 200 mA. The scan range was $20^{o} < 2\theta < 80^{o}$ at 2^{o} min^{-1}.High resolution powder diffraction (HRPD) was carried out in 9B beamline of Pohang Light Source-II (PLS-II, 3 GeV). The incident beam was a wavelength of 1.5490 Å using a double-crystal Si (111) monochromater. A scan range of 2θ was $15^{o} < 2\theta < 135^{o}$ with 0.02^{o} increments and 0.5^{o} overlaps to the next detector.

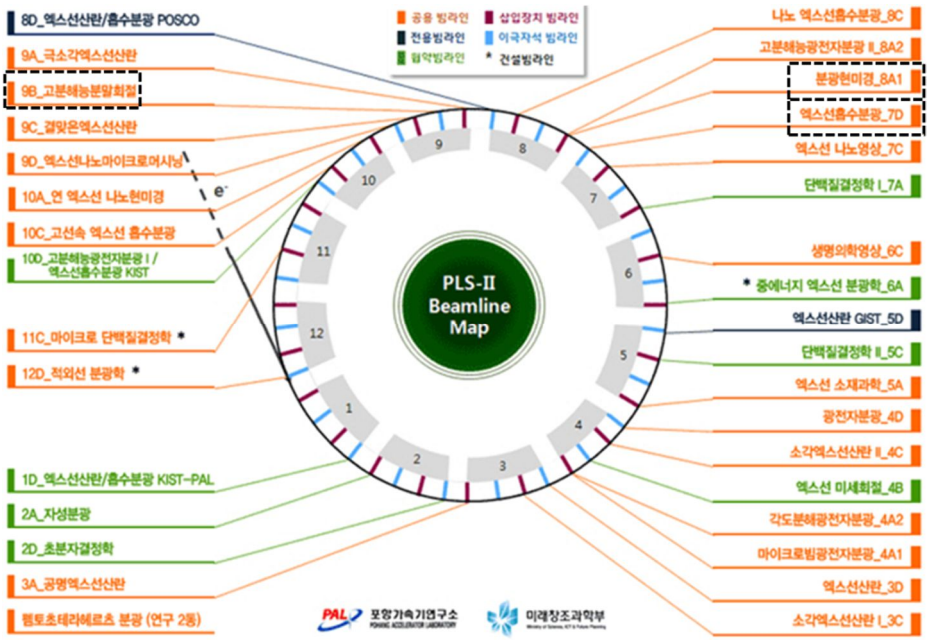

Figure 2.1. Beamline map in the Pohang Accelerating Laboratory (PAL) (http:// pal.postech.ac.kr)

X-ray photoelectron spectroscopy (XPS) was measured using Thermo Sigma Probe with Al Kα radiation. All spectra were calibrated with the C-C peak of C 1s orbitals as 284.6 eV. The peaks were fitted by XPSPEAK 4.1 software package.

To analysis quantitative information, inductively coupled plasma-atomic emission spectroscopy (ICP-AES, Sumdzu, JP/ICPS-7500) and elemental analysis (EA, LECO corp. US/CHNS-932) were conducted.

X-ray absorption near edge structure (XANES) measurement was carried out in 7D beam line of Pohang Light Source-II (PLS-II, 3 GeV). The incident beam was monochromatized using a Si (111) double crystal monochromator and detuned by 15 % to minimize the unwanted higher harmonics, in particular, the third order reflection of the silicon crystals. All spectra were taken in a transmission mode with separate He-filled IC Spec ionization chambers for incident and transmitted beams, respectively. Before measuring samples, energy calibration was conducted with a reference Pt or Au foil. The energy scan was performed in five regions for good energy resolution in a steep absorption and measurement of XANES and EXAFS spectra at a time. The obtained data were processed in the usual way to obtain the absorbance and analyzed with ATHENA and ARTEMIS in the suite of IFEFFIT software programs. Pre-edge absorption due to the

background and detector were subtracted using a linear fit to the data in the range of -200 to -50 eV relative to E_0. E0 was defined as the first inflection point on the rising absorption edge. Each spectrum was then normalized by a constant, extrapolated value to E0 of third –order polynomial fit over absorption. To isolate EXAFS signal, the post-edge background function was approximated with a piecewise spline that could be adjusted so that the low-R component of pre-Fourier transformed data were minimized.

2.1.5. Electrochemical measurements

The three electrode cell was used to characterize the electrochemical measurement of carbon supported catalyst; working electrode (catalyst ink on a glassy carbon electrode), reference electrode (saturated calomel electrode, SCE), and counter electrode (Pt wire). All measurements were performed using an AUTOLAB potentiostat (Eco Chemie, PGSTAT) at 20 ^{o}C. Potentials were referred as a reversible hydrogen electrode (RHE) to calibrate hydrogen oxidation calibration method. To compare Pt nanoparticles, a commercial carbon supported Pt, denoted as Pt/C, was used as a reference (Johnson Matthey 40 wt.%). A catalyst ink composed of 0.001 g of the catalyst, 800 μL of methanol, and 59.2 μL of Nafion solution. Catalyst ink was transferred to glassy carbon electrode after sonication to

obtain homogeneous solution. To confirm electrochemical stability, pre-potential cycling was carried out at a potential between 0.05 and 1.0 V with a scan rate, 50 mV s^{-1}. All electrochemical measurements were performed in 0.1 M $HClO_4$ except for the CO electro-oxidation reaction in 0.5 M H_2SO_4.

2.1.6. CO stripping and oxygen reduction reactions

CO stripping measurement was performed after the completion of adsorption of CO at 0.5 V with a high purity CO gas (99.99+%). Cyclic voltammograms (CV) of CO oxidation curves was acquired in 0.1M $HClO_4$ with a scan rate, 20 mV s^{-1}, after removal of residual CO gas into Ar. The electrode was washed with deionized water and put into the electrochemical cells. The CVs were obtained from the modified electrocatalysts. The experimental details were described in Supporting Information. Polarization curves for the oxygen reduction reaction (ORR) were conducted using rotating disc electrode (RDE) in 0.1 M $HClO_4$ with a saturated O_2 (99.995%) at a scan rate and rotating speed, 5 mV s^{-1} and 1600 rpm, respectively. The kinetic current density of the ORR was calculated by the equation;

$$\frac{1}{j} = \frac{i}{j_L} + \frac{1}{j_k}$$

where, j, j_L, and j_k are measured, cathodic limiting, and kinetic current density, respectively. Polarization curves were corrected by the blank CV, measured with the same condition of the ORR except for Ar-saturated atmosphere. Specific or mass activity (vs. Pt/C) was defined as the extent of enhancement of the specific or mass kinetic current density (j_k) toward Pt/C at 0.9 V.

Chapter 3. Results and Discussion

3.1. Electronic and geometric structures of Au/Pt nanoparticles

3.1.1. Synthesis and morphology

Conventional TEM was used to inspect the samples for their size and distributions of nanoparticles. The TEM image showed that the Au/C nanoparticles were reasonably well dispersed and spherical shaped with average diameters of 3-4 nm for Figure 1. After the deposition of Pt shell through hydroquinone (HQ) method, the size of samples was monotonically increased. Each sample was well dispersed without the agglomeration of nanoparticles and small size of nanoparticles. From these TEM image, the core-shell like nanoparticles were well achieved. These findings indicate that this HQ assisted reduction method is optimal for production of core-shell nanoparticles due to the mild reduction ability.[57]

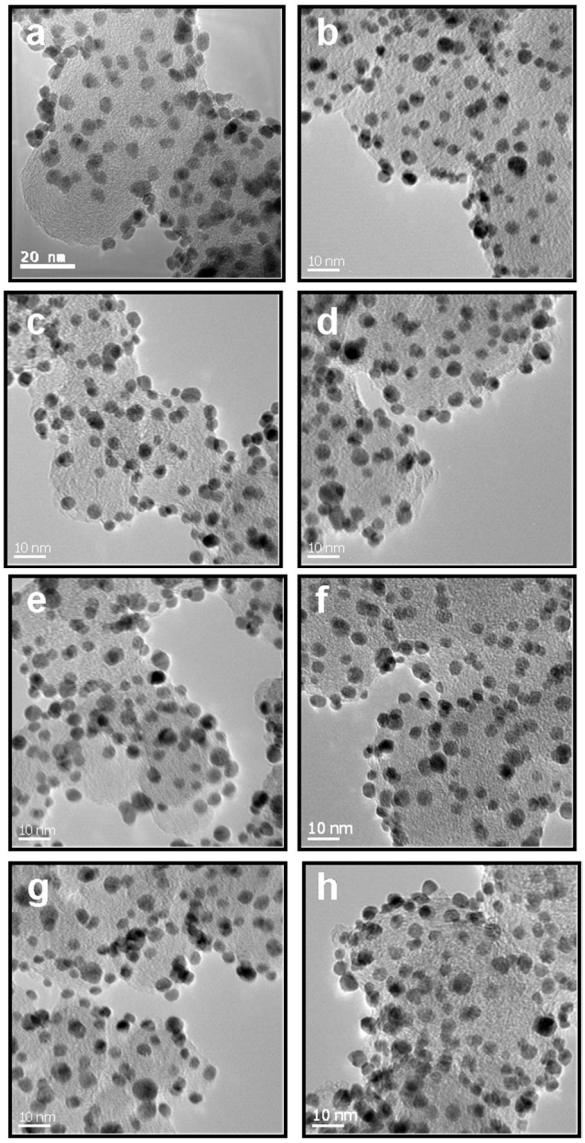

Figure 3.1. Normal TEM images of Au@Pt_x nanoparticles (a:Au/C, b: Au@Pt_0.02, c: Au@Pt_0.10, d: Au@Pt_0.20, e: Au@Pt_0.30, f: Au@Pt_0.50, g: Au@Pt_0.50 and h: Au@Pt_0.65)

Conventional TEM analysis provide insufficient atomic configuration for determination of core-shell nanoparticles due to the aberration issues. Therefore, aberration corrected TEM and STEM with a high angle annular dark field (HAADF) detector were used to confirm the core-shell structure. Aberration corrected HR-TEM image showed that Au@Pt_xnanoparticles were well synthesized with epitaxial growth. Due to the similar lattice parameter for Au and Pt, any difference was not clearly confirmed. Generally, the atoms deposited to the core particles as different scheme. The first mechanism is Frank-van der Merwe type, which the sum of the shell and interface free energy is smaller than the core free energy. However the Volmer-Weber type which the island was formed with deposition of shell materials because free energy of core materials is lower than that of the shell materials.[59] In case of Au and Pt, the surface free energy of Au at room temperature is 1.63 J m^{-2} and the Pt is2.69 J m^{-2}.[60] Due to the thermodynamic concerns, outer Pt shell was formed Volmer – Weber type which island formed. Because the size of Au@Pt_x samples was extremely small with 4 – 5 nm, we could not confirm the exact atomic configuration of Pt. However the particles were shown that well deposited. To clearly confirm the core-shell structure, the HADDF STEM analysis was conducted. The HADDF STEM intensity is directly related to the square of the atomic

number of the elements, making the Au atoms appear bright relative to Pt theoretically. However, the atomic number difference of Au and Pt is only 1. Due to the very similar atomic number, the difference was not clearly shown. The energy dispersive spectrometer (EDS) analysis clearly showed the core-shell structure. The outer Pt shell thickness was around 0.5 nm which the Pt shell is around 1-2 layers. Aberration corrected TEM image also clearly verified the core-shell structure. From the fast Fourier transformation (FFT) images, we confirmed the split of Au@Pt (111) peak. We investigated the FFT pattern using masking method and then inverse Fourier transformation. Each inverse Fourier transformed image showed the core and shell, respectively. The atomic distance of inverse Fourier transformation image is directly correlated to the core as Au (111) and shell as Pt (111).

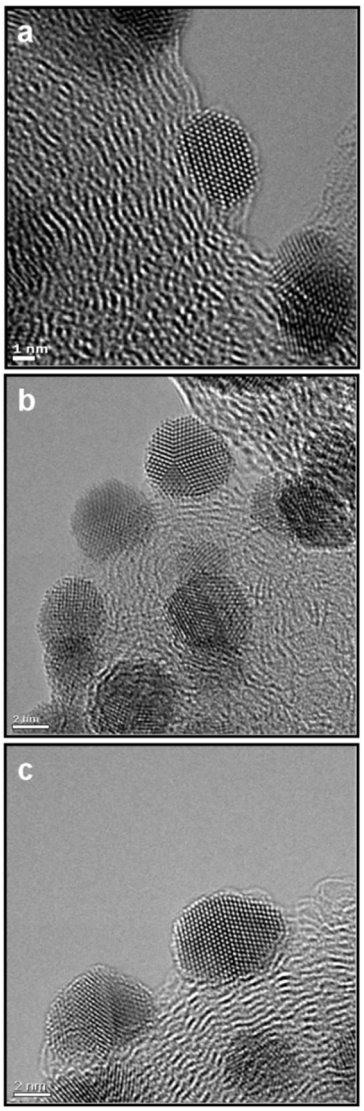

Figure 3.2. Aberration Cs-corrected HR-TEM images of (a) Au/C, (b) Au@Pt_0.3 and (c) Au@Pt_0.65.

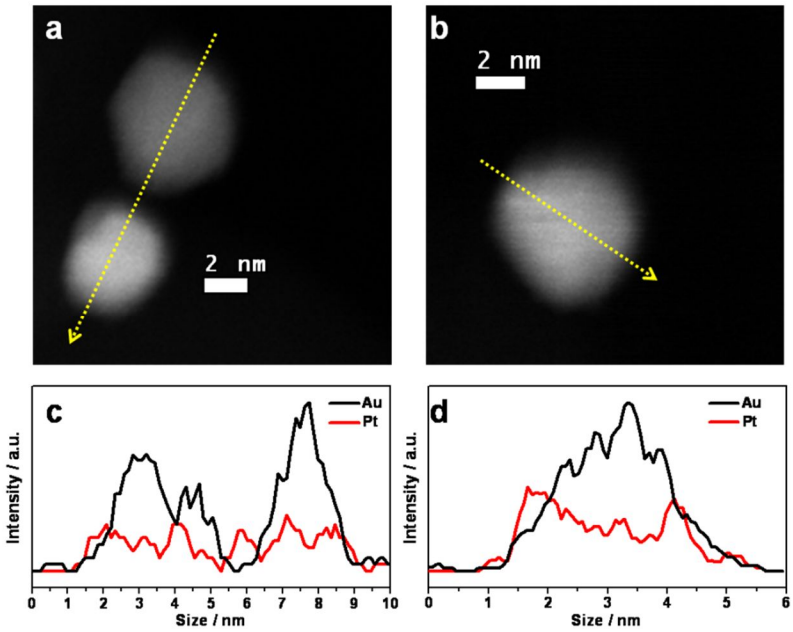

Figure 3.3. HAADF STEM images and their EDX line scan results (a,c : Au@Pt_0.3 and b,d: Au@Pt_0.65)

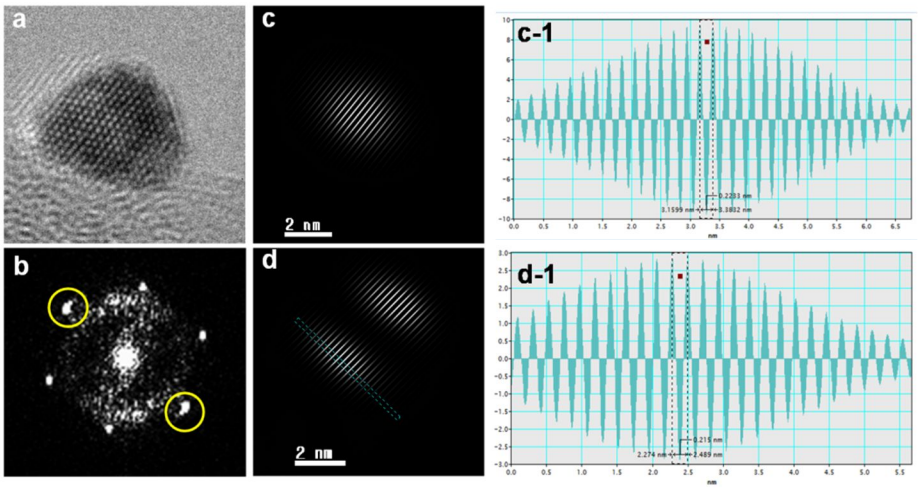

Figure 3.4. Aberration Cs-corrected HR-TEM images, their FFT patterns, inverse Fourier transformation images after masking and atomic distance of Au@Pt_0.50.

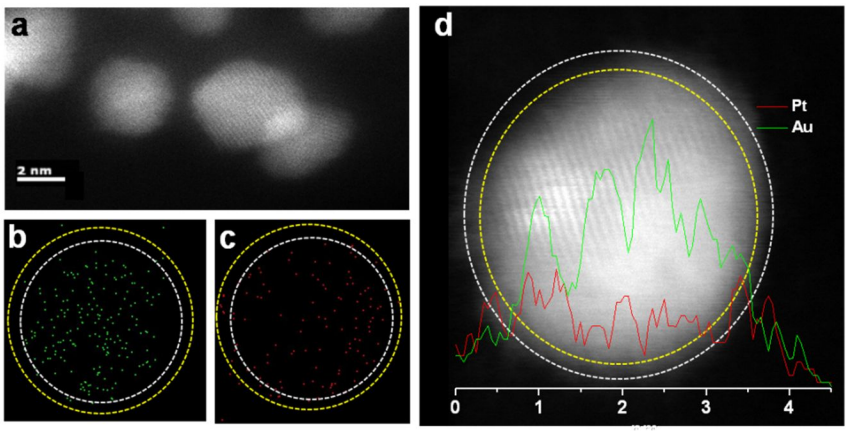

Figure 3.5. Aberration Cs-corrected HADDF-STEM images and EDX mapping and line scan results of Au@Pt_0.5.

The AuPt alloy nanoparticles were also well made confirmed by the TEM. The size of AuPt alloy nanoparticles was slightly smaller than that of the core-shell nanoparticle.

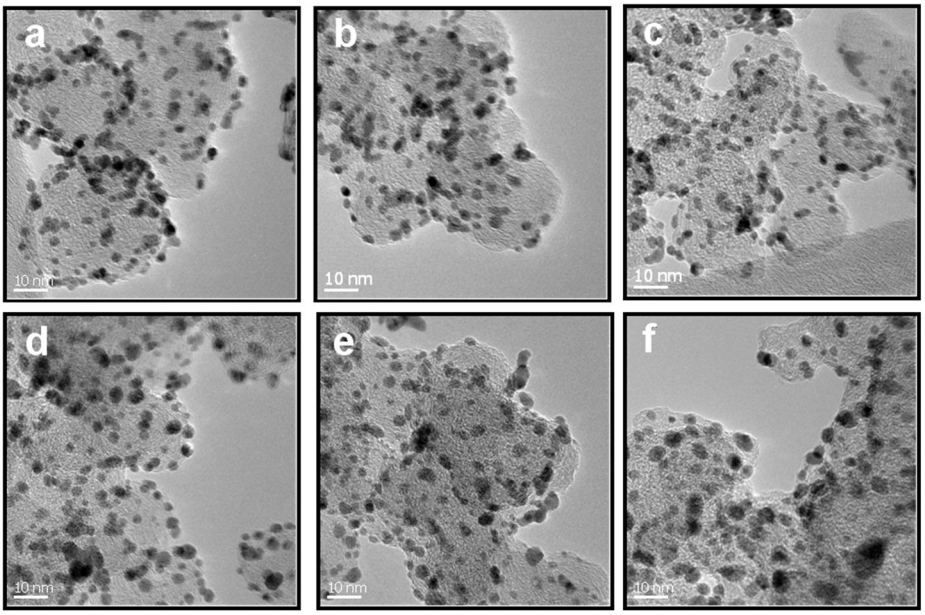

Figure 3.6. Normal TEM image of AuPt alloy nanoparticles. (a: Au1Pt3.5, b: Au1Pt2.25, c: Au1Pt1.5 d: Au1Pt0.75, e: Au1Pt0.5 and f: Au1Pt0.25)

Table 3.1.Summary of compositions and TEM analysis.

Catalysts	Pt/Au (ICP)	Pt/Au (XAFS)[a]	Size (TEM)[b] /nm	Standard deviation /nm	Estimated size[c] / nm
Au			3.58	0.39	-
Au@Pt_0.02	0.02	0.02	3.60	0.70	3.63
Au@Pt_0.10	0.11	0.10	3.68	0.72	3.71
Au@Pt_0.15	0.15	0.16	3.70	0.68	3.77
Au@Pt_0.20	0.20	0.21	3.75	0.71	3.81
Au@Pt_0.30	0.31	0.28	3.93	0.64	3.91
Au@Pt_0.50	0.51	0.48	4.25	0.75	4.09
Au@Pt_0.65	0.64	0.63	4.40	0.81	4.19
Au1Pt0.25	0.24	0.24	3.68	0.73	-
Au1Pt0.5	0.50	0.47	3.38	0.78	-
Au1Pt0.75	0.77	0.75	3.37	0.78	-
Au1Pt1.5	1.48	1.56	3.06	0.67	-
Au1Pt2.25	2.28	2.27	3.11	0.67	-
Au1Pt3.5	3.44	3.45	3.06	0.75	-

[a] Pt/Au from XAFS was calculated by the edge jump ratio in Pt L_3 edge after normalization

[b] Size by TEM was counted 50 particles from TEM images

[c] Estimated size was calculated using Equation

$$d_{Au@Pt} = [(\frac{n_{Pt}}{n_{Au}})(\frac{V_{Pt}}{V_{Au}}) +]^{1/3} d_{Au}$$

V_{Pt}/V_{Au} =0.89,

(Pt atomic radius 139pm))

3.1.2. Structure characterizations

To confirm the core-shell structure of Au@Pt_x nanoparticles, synchrotron base photoelectron spectroscopy (PES) was used. PES is very powerful techniques. However, in nanoparticle analysis, the impurity can affect the signal. Generally, three methods are possible to investigate core-shell structure using PES. The first one is depth profiling using sputter. By etching the structure using Ar sputtering, the depth profile analysis can analyze the structure. The second method is using characteristics of electron. The degree of surface sensitivity of an electron-based technique may be varied by collecting photoelectrons emitted at different emission angles to the surface plane. However the most powerful method is photon energy dependent measurement using only synchrotron facilities. The probability of escape from a given depth, P(d) is determined by the probability of the electron not being inelastically scattered during its projection to the surface. The probability is related to the Inelastic Mean Free Path (IMFP) of electrons. IMFP means the average distance projected by an electron through a solid before it is inelastically scattered. IMFP depends on the two parameters. The first is the nature of solid itself. However in most cases, this term is almost same. The second term is the initial kinetic energy of electron which is determined by the incident photon energy. As shown in

equation, probability of escape (P(d)) is function of electron travelling distance (d) and λ which is related to the IMFP.

$$P(d) = \exp(-d/\lambda)$$

IMFP is generally showed on a log scale plot because log scale can show the tendency of whole range more clearly. The universal curves are shown in Figure. From the universal curves, the IMFP increased as kinetic energy increased from the about 50 eV. At lower energies, the probability of inelastic scattering decrease since the electron has insufficient energy to cause plasmon excitation. By using synchrotron PES, the incident photon energy can be easily controlled. Considering the binding energy of Pt $4f_{7/2}$ (71.2 eV) and Au $4f_{7/2}$ (84 eV), the minimum IMFP is the range of 130 eV. The Pt 4f and Au 4f spectra were measured under the 130, 320, 510, 630 and 750 eV. Before the each measurement, the energy was calibrated using Au foil Au $4f_{7/2}$ and Fermi edge of Au. To confirm the bulk ratio of samples, lab sources (Al Kα, 1486 eV) X-ray photoemission spectroscopy was measured. The area ratio of Au : Pt is about 1 : 0.5 which is well matched with ICP analysis and XAFS analysis. The area ratio of incident photon energy was compared and plotted as shown in Figure. Bulk composition

ratio of Pt/Au is about 4 in 130 eV. By increasing the photon energy, the area ratio Pt/Au decreased. If the structure is homogenous alloy or mixture, the photon energy dependent area should be same. The measured trends also confirmed the core-shell structure of Au@Pt_x nanoparticles.

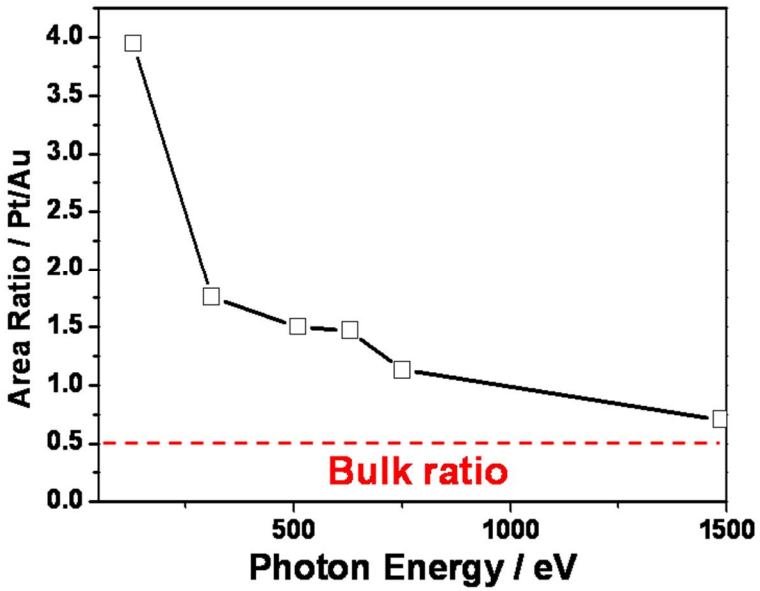

Figure 3.7. High resolution photo emission spectroscopy (HR-PES) results under different photon energy to confirm the core-shell structures of Au@Pt_0.5.

X-ray diffraction analysis was conducted to investigate the lattice parameter change. In alloy nanoparticle, their lattice parameter changed by the composition of Au and Pt. As Pt ratio increased, the lattice parameter decreased. From the Vegard's law, we compared the theoretical lattice parameter and measured ones. The lattice parameter was larger than that of the expected values from the Vegard's law. It meant that the degree of alloying is rather small compared to expected atomic ratio. The relatively low degree of alloying was related to the synthesis environment and the surface free energy of two atoms. The first reason is maybe related to the synthesis temperature. Alloy nanoparticles were synthesized room temperature. However, the standard reduction potential of Au is higher than that of the Pt. It means that the Au reduction is facile compared to the Pt. Due to the low temperature, atomic diffusion is slow. These reasons may contribute the core Au rich and shell Pt rich alloy phase. Second possible reason is the surface free energy. The surface free energy of Au is much lower than that of the Pt. These parameters contribute to the surface composition change. To exact confirm the atomic configuration, the more detailed analysis was required.

In case of Au@Pt nanoparticle, the XRD features were not changed by composition change. Only the peak shape changed. Note that usually a

heterogeneous core-shell structure would have broad overlaying peaks of two sets of diffraction peaks from each component in XRD. The components should have comparable amount in the whole nanostructures, as otherwise the dominant phase would bury the features of the minor phase.[61] A clear boundary at the interface would also be important for observing the overlaying peak, where mixed phase at the interface would give XRD peaks between respective peaks of each component.[62]Due to clearly investigate the Pt lattice parameter, very accurate measurement was required. Synchrotron based high resolution powder diffraction was conducted at PAL. The angle error is below the 0.0001 which is one of the most accurate values. The HRPD results showed that the peak shape changed from the symmetric to asymmetric by increasing the deposition of Pt amount. However, the lattice parameter of Pt is not calculated by the peak itself.

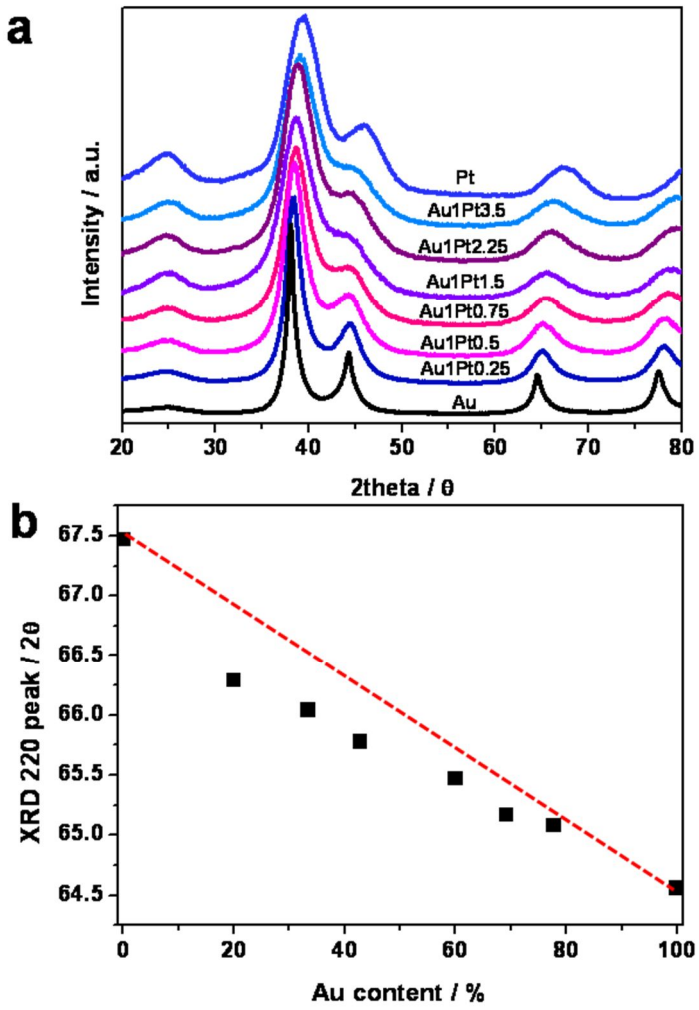

Figure 3.8.XRD analysis of Alloy AuPt nanoparticles.

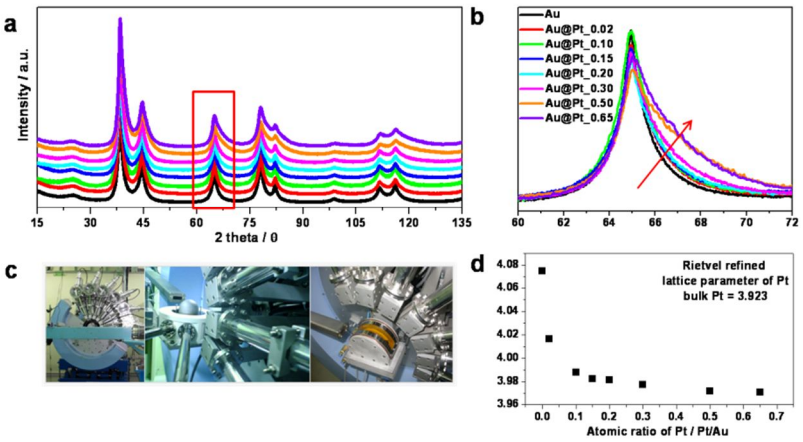

Figure 3.9.HRPD analysis of core-shell Au@Pt nanoparticles and theirRietveld analysis results.

To confirm the delicate lattice parameter of Pt, the whole pattern matching profile method was used. The core Au nanoparticle was measured and calculated the lattice parameter from whole pattern profile matching. The core information through the whole pattern profile matching was used as parameter for whole pattern profile matching of Au@Pt nanoparticle. By fixing the core parameter, whole pattern profile matching was conducted. During the deposition of Pt atom to core Au, the Pt atom may affect the lattice parameter of Au by strain effect. However the strain effect was disregarded by considering that the effect was only confined to surface. By increasing the Pt deposition amount, degree of asymmetric increased and the Pt lattice parameter decreased.

The amount of lattice strain effect was calculated by the Pt lattice parameter. Due to the larger atomic size of Au, the Pt was affected by the tensile strength. The strain effect was decreased by the increasing the Pt deposition.

From the XRD analysis, we could get information related to the long range ordering. In the case of nanoparticles, the local information is very important to determine materials its own properties. XAFS was measured at PAL 7D beamline. The Au L_3 edge (11,919 eV) and Pt L_3 edge (11,564 eV) were measured. To analysis the EXAFS spectra, minimum 10 K is required, however the Au L_3 edge is overlapped with the Pt L_3 edge EXAFS signal

unfortunately. EXAFS analysis of Au/Pt system is also one of the difficult systems due to the same crystal structure and relatively same atomic radius and backscattered factor. Due to the complex system, delicate analysis should be required. Local structure of nanoparticles was examined through the Au L_3 edge signals. The EXAFS analysis was conducted by assuming that the Au and Pt signals are almost same, because it is difficult to separate the information between Au-Au and Au-Pt term. The information related to the Au-M (Au or Pt) was obtained by fitting. The obtained data were processed in the usual way to obtain the absorbance and analyzed with ATHENA and ARTEMIS in the suite of IFEFFIT software programs. To isolate the EXAFS signal, the post-edge background function was approximated with a piecewise spline that could be adjusted so that the low-R component of pre-Fourier transformed data was minimized. After calculation of EXAFS function, k^3-weighted EXAFS function in momentum (k) space was Fourier transformed to reveal the neighboring atoms arranged according to the distance from a central atom in R-space. The k range of the transform varied between a k_{min} of 2.0–3.0 A 1 and a k_{max} of 12.0–13.0A 1. The Kaiser–Bessel function was adopted as a window function and the windowsill of dk ¼ 1.0 was also used in the transform. A shell of interest in R-space was backtransformed into the momentum space with the Kaiser–

Bessel window function and a windowsill of dR ¼ 0.5. Fourier-filtered spectra derived from the experiments were fitted by using the theoretical standards generated with the ab initio FEFF 8.2 code.

In the case of Au@Pt nanoparticles, the Au-M distance decreased by increasing the amount of Pt deposition.[63] Even though the amount of the Pt deposition was increased, the Au-M range was little changed. These results also verified that structure Au@Pt nanoparticles was phase segregated such as core-shell structure. The coordination number increased as Pt deposited. In the case of alloy nanoparticles, the change ofAu-M distance was clearly shown. By increasing the Pt composition, the Au-M decreased. This result was well explained that the structure of AuPt alloy nanoparticles which were well mixed. However the structure was off the point exact homogeneous phase which was also confirmed in XRD study. Due to the different standard reduction potentials and the temperature, the shell part was dominant in Pt phase. To clearly show the structure difference by EXAFS study, we plotted the Au content over R_{Au-M}.

Dotted line was calculated the theory which the distance of Au-M is direct composition related functions. From the equation, even though the partial distance R_{Pt-Pt}, R_{Au-Au} and R_{Pt-Au}= R_{Au-Pt} cannot be obtained from the analysis for the systems. They are expected to increase monotonically with Au

composition. R_{Au-Au} was directly measured with the Au/C nanoparticles, however, the R_{Au-Pt} was not measured which was ideal cases. The R_{Au-Pt} was estimated from the half value of R_{Pt-Pt} and R_{Au-Au}.

The estimated values are deviated from the real values however, the relationship was not changed. In the case of the alloy nanoparticles, the trend of R_{Au-M} was well correlated to the expected guideline which was based on the homogeneous phase. However, in the case of core-shell nanoparticles, their R_{Au-M} was little changed and was the range of pure Au. These results showed that the core-shell nanoparticles was compromised Au segregated which was direct evidence of core-shell structure.

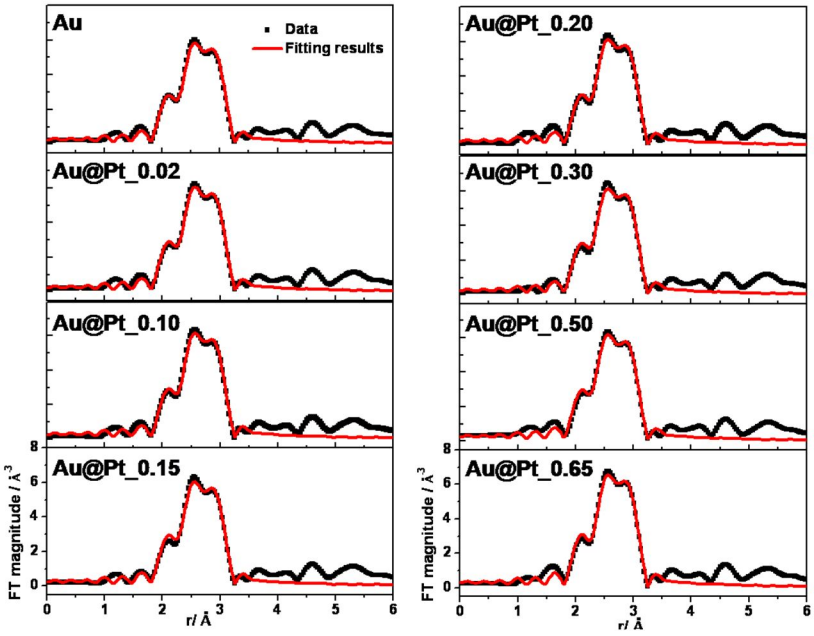

Figure 3.10. Au L3 EXAFS spectra of Au@Pt nanoparticles.

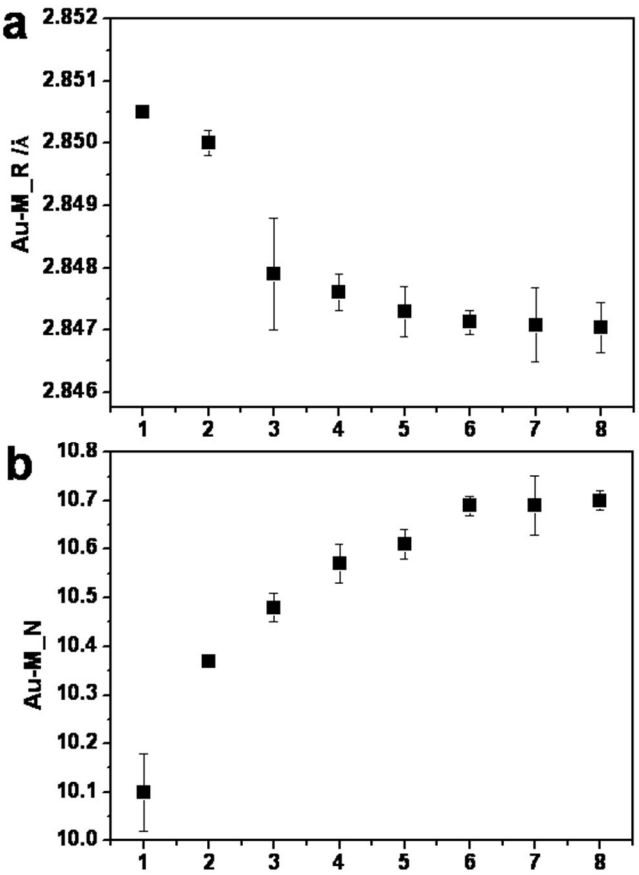

Figure 3.11. Au L3 EXAFS results of Au@Pt nanoparticles. (a) Au-M distance results from fitting and (b) coordination numbers. (1:Au/C, 2: Au@Pt_0.02, 3: Au@Pt_0.10, 4: Au@Pt_0.20, 5: Au@Pt_0.30, 6: Au@Pt_0.50, 7: Au@Pt_0.50 and 8: Au@Pt_0.65)

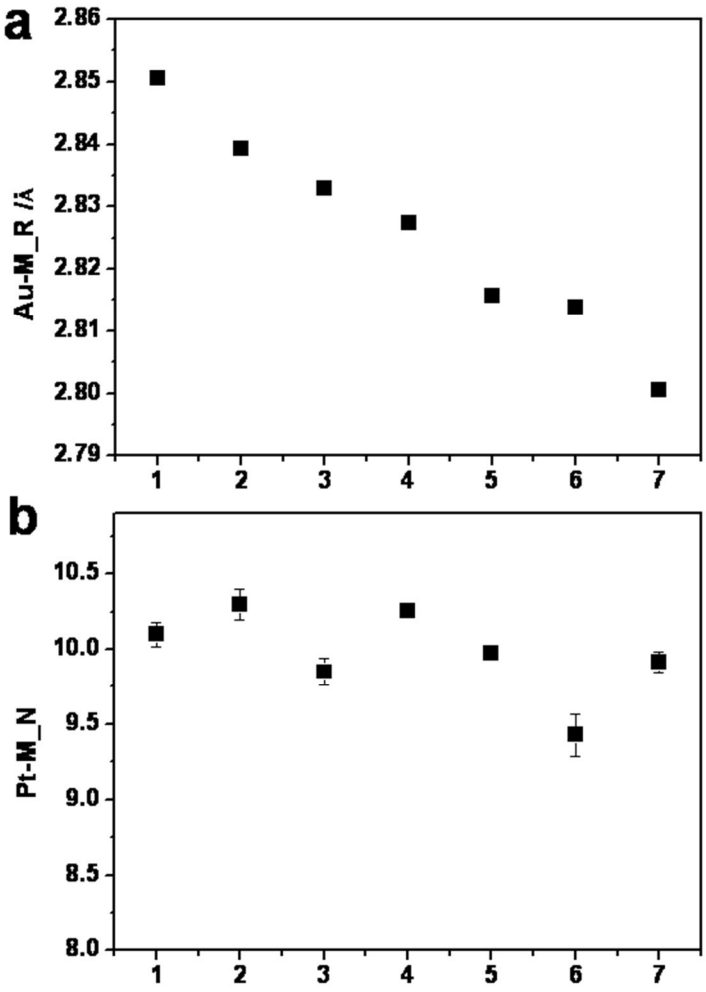

Figure 3.12. Au L3 EXAFS results of AuPt alloy nanoparticles. (a) Au-M distance results from fitting and (b) coordination numbers. (1: Au/C, 2: a: Au1Pt3.5, 3: Au1Pt2.25, 4: Au1Pt1.5 5: Au1Pt0.75, 6: Au1Pt0.5 and 7: Au1Pt0.25)

Table 3.2. Summary of EXAFS analysis

Catalysts	Au-M /Å	Coordination number / N	Debye-waller factor /Å^2	R factor
Au	2.8505(2)	10.1	0.0085	0.0053
Au@Pt_0.02	2.8500(7)	10.4	0.0085	0.0065
Au@Pt_0.10	2.8479(5)	10.5	0.0084	0.0061
Au@Pt_0.15	2.8476(1)	10.6	0.0087	0.0074
Au@Pt_0.20	2.8473(1)	10.6	0.0084	0.0087
Au@Pt_0.30	2.8471(2)	10.7	0.0086	0.0057
Au@Pt_0.50	2.8470(8)	10.7	0.0084	0.0098
Au@Pt_0.65	2.8470(4)	10.7	0.0082	0.0100
Au1Pt0.25	2.8006(1)	9.9	0.0087	0.0016
Au1Pt0.5	2.8138(6)	9.4	0.0092	0.0131
Au1Pt0.75	2.8156(7)	10.0	0.0090	0.0049
Au1Pt1.5	2.8274(2)	10.3	0.0100	0.0075
Au1Pt2.25	2.8329(3)	9.9	0.0089	0.0048
Au1Pt3.5	2.8393(1)	10.3	0.0054	0.0145

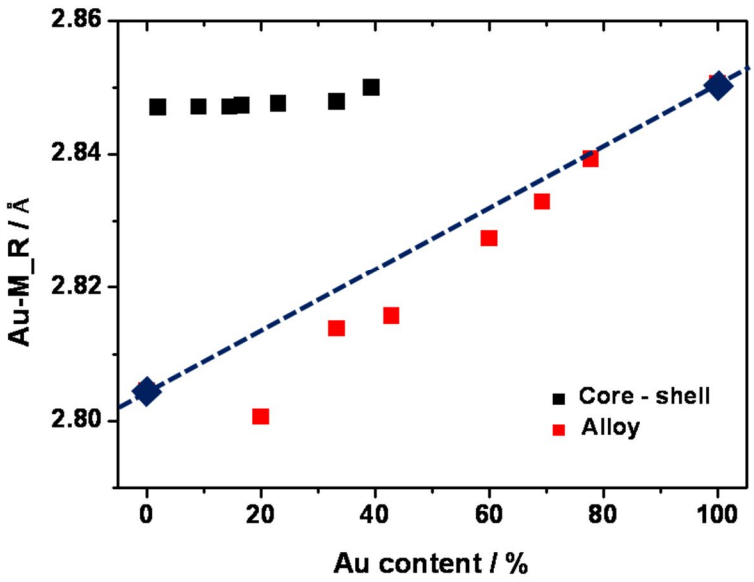

Figure 3.13.Au L3 EXAFS analysis summary and the structure dependence of Au-M.

3.1.3. Electrochemical measurements

The surface composition ratio between Au and Pt can be estimated from electrochemical method. The first method is comparing the Au and Pt oxide reduction peak from the CV. Au oxide reduction peak range is from the 1.0 to 1.3 V_{RHE} and Pt oxide reduction peak range is 1.0 ~ 0.7 V_{RHE}. The measured charge is normalized the each known parameter which the Pt oxide is normalized with the 420 μCcm^{-2} and Au oxide is normalized with the 210μCcm^{-2}. From these values, the surface Pt ratio can be estimated.[64] However these values has many errors because, the Pt oxide is not formed with monolayer. The other method is Pt composition was calculated from the H_{upd} (Hydrogen underpotential deposition). In general cases, the Pt area calculated by H_{upd} is reasonable, however, there also has uncertainty. D. vanderVliet reported that the H_{upd} was affected by the ligand effect.[65]Furthermore, the determination of the surface area via the H_{upd} charge corrected by a constant double layer capacity is flawed by a systematic error. This conventional background correction has critical weakness in high surface catalyst with carbon support. To calculate the more exact Pt surface area is CO stripping method (CO electro-oxidation method). CV in Ar purged solution is compared to a CO bulk oxidation curve. Final method to estimate the whole surface area is Cu underpotential method. The

conversion factor of 420 $\mu Ccm^{-2}$is then typically used to evaluate the surface area of Pt or Au nanoparticles which is assumed that a one-to-one correspondence between Au or Pt atoms and Cu atoms. Proper correction for the stoichiometry of the reaction can be used to find the total number of platinum atoms by H_{upd} and CO stripping and the total number of Au and Pt atoms on the surface of the nanoparticles. However, Cu underpotential method has also systematic error. Exact surface composition of Pt is not easily allowed. Comparing the area of charge of CO stripping and Au oxide reduction peak was used in this report. The Pt area was calculated from the CO stripping measurement and calibrated the background as Ar purged cases. The Au area was measured CV which was measured to 1.6 V_{RHE}. As expected, as increasing the Pt amount the surface composition of Pt increased. In the case of core-shell nanoparticles, the surface was not fully covered with the Pt. In the case of alloy nanoparticles, the surface composition of Pt is larger than that of the bulk composition which reflected the surface Pt richness.

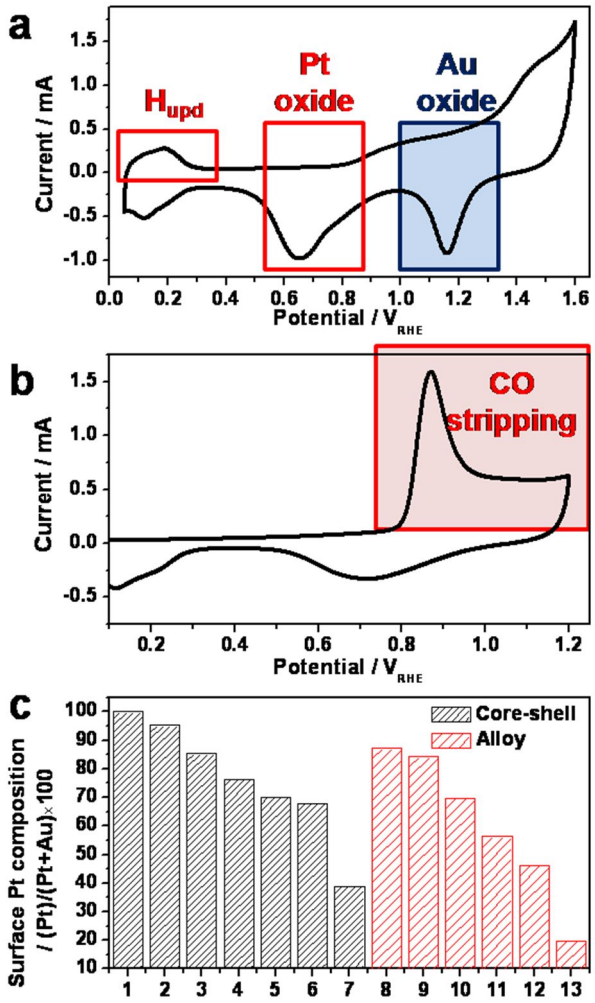

Figure 3.14.(a) Cyclic voltammograms of Au@Pt_0.2 nanoparticles and their CO stripping results and (c) surface Pt compositions. (1:Pt/C, 2: Au@Pt_0.10, 3: Au@Pt_0.20, 4: Au@Pt_0.30, 5: Au@Pt_0.50, 6: Au@Pt_0.50, 7: Au@Pt_0.65, 8: Au1Pt3.5, 9: Au1Pt2.25, 10: Au1Pt1.5 11: Au1Pt0.75, 12: Au1Pt0.5 and 13: Au1Pt0.25)

Comparing the strength between metal and OH species is hard and not suitable in different Pt surface composition cases. To compare, the strength between Pt and CO was used. CO was the neutral prove for measuring the adsorbate-metal interaction. It has been reported that the linear relationship between OH and CO to metal. By examining the CO binding strength, the Pt-OH interaction tendency may be conducted.[66] CO electro-oxidation has been studied many years.[67] However the exact mechanisms are under debate. Many research suggested that the Langmuir-Hinshelwood mechanism, in which oxidation of H_2O generates chemisorbed OH. This process is then followed by a reaction between adsorbed OH (OH_{ad}) and adsorbed CO (CO_{ad}).[68]

$$H2O + Pt \rightarrow Pt\text{-}OH_{ad} + H^+ + e^-$$

$$Pt\text{-}CO_{ad} + Pt\text{-}OH_{ad} \rightarrow CO_2 + 2Pt + H^+ + e^-$$

In general, the CO stripping peak potential on Pt catalyst correlates directly with the Pt d-band center.[69-72]A highly lying Pt d-band center can lead to a strong CO adsorption due to a decreased electron back donation from Pt to the antibonding orbitals of CO molecules. CO stripping peak position of core-shell Au@Pt nanoparticles shifted steadily to lower potentials with increasing the amount of Pt deposition.[73][74] However, the peak position of Au@Pt_0.65, Au@Pt_0.50 and Au@Pt_0.30 samples was lower

than that of the pure Pt.[75] It was intriguing results that Pt in Au@Ptstructure has strong interaction with CO due to the tensile strength. Conventional Ab-initio model predicted that if larger atoms were embedded in the structure, the tensile strength increased. From the d band model, tensile strength induced the small orbital overlap which induced the band-shape reconstruction. With the narrow bandwidth, the center of d-band which is the general strength parameter between d metal and adsorbate increased or up shifted. D-band center up shift means that metal adsorb the adsorbate strongly. As Pt deposited to the Au surface, the tensile strength which Pt was affected was decreased. However, the tensile strength does not disappear all the samples as confirmed in the HRPD analysis. From the Rietveld analysis, the lattice parameter of Pt decreased as increasing the Pt amount. However, 1.2 % of strain was still remained in Au@Pt_0.65 samples which are smallest lattice parameters in core-shell samples. The conventional d-band center model does not explain our data. This trend also confirmed in surface Pt rich alloy nanoparticle. The extent of position shift was relatively smaller than the core-shell structure. However, the position of Au1Pt3.5 is 0.2 V_{RHE} smaller than that of the Pt.

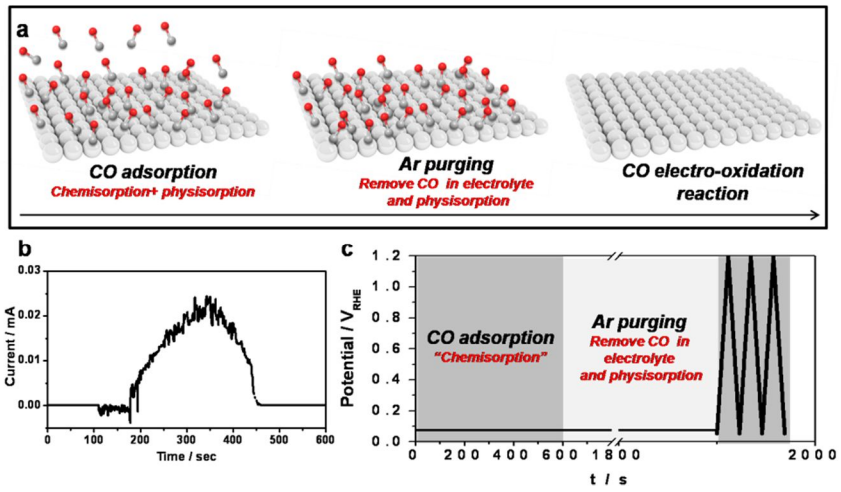

Figure 3.15.(a)CO stripping schemes, (b) CO adsorption charge and (c) CO stripping method

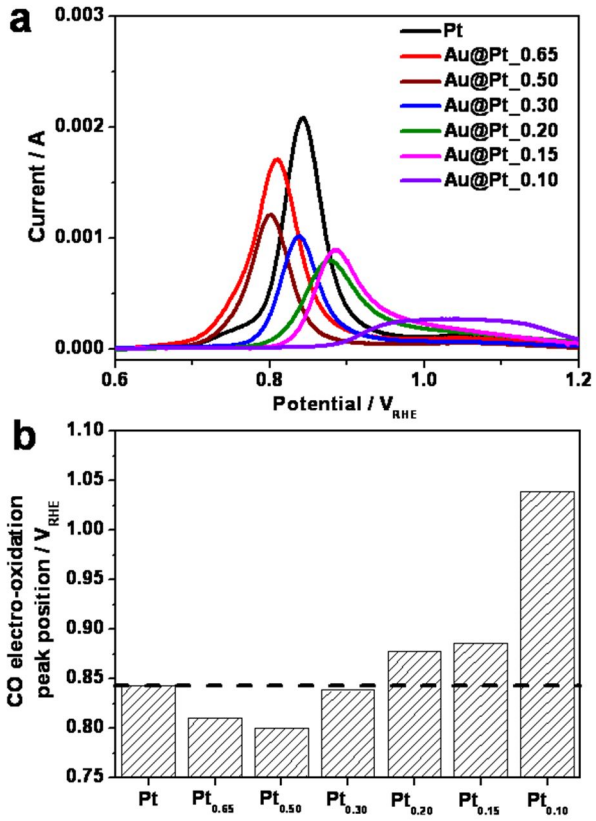

Figure 3.16.(a)CO stripping results of Au@Pt and (b) CO electro-oxidation peak potential.

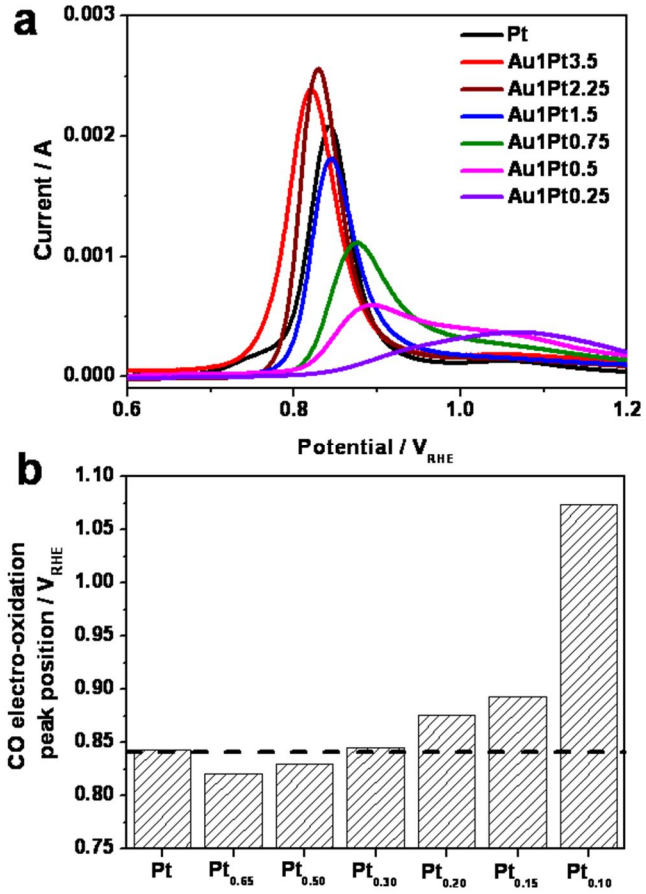

Figure 3.17.(a)CO stripping results of AuPt and (b) CO electro-oxidation peak potential.

To confirm the trends, the potential of zero total charge (PZTC) was also conducted. The PZTC is the potential at which excess charge density becomes equal to the charge density transferred during the adsorption. Therefore, the PZTC depends on surface properties such as the work function and surface geometry of the electrode. The measured PZTC values were reasonable compared to those in previous reports. The relation between charges for the calculation of PZTC can be obtained by integrating the voltammetric curves using charges displaced by CO as integration constants, which are measured by integrating the current time transients at 0.075 V_{RHE} using the following the equation:

$$Q = \int_{0.075\ V}^{E} \frac{\rceil j \lceil}{\upsilon} dE \ - q_{dis}\,(0.075\ V)$$

where j is the voltammetric current, υ is the sweep rate, and q_{dis} is the charge displaced at a certain potential, which is 0.075 V in our case. The PZTC trends are correlated to the oxophilicity. The higher PZTC means the low oxophilicity. From the PZTC, the trend of Pt-CO was same with the Pt-OH because oxophilicity is related to the Pt-OH interaction strength.

From the CO stripping method and PZTC, the composition dependent strength change was confirmed. To explain the intriguing phenomena, theoretical views was required. Detail considerations are as follows,[76, 77]

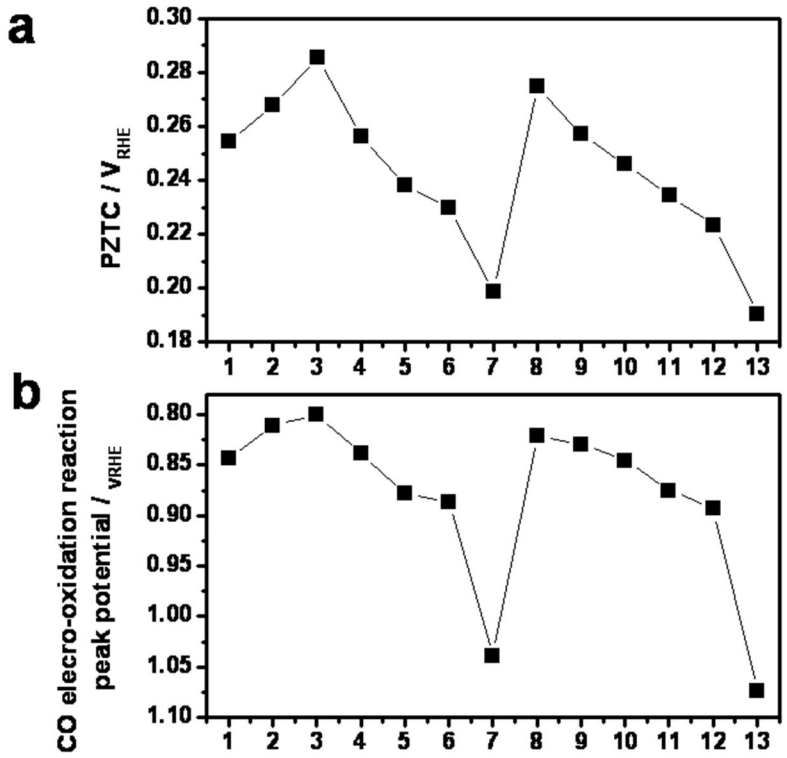

Figure 3.18.(a)PZTC resultsof AuPt and (b) CO electro-oxidation peak potential.(1:Pt/C, 2: Au@Pt_0.10, 3: Au@Pt_0.20, 4: Au@Pt_0.30, 5: Au@Pt_0.50, 6: Au@Pt_0.50, 7: Au@Pt_0.65, 8: Au1Pt3.5, 9: Au1Pt2.25, 10: Au1Pt1.5 11: Au1Pt0.75, 12: Au1Pt0.5 and 13: Au1Pt0.25)

Chemisorption of OH and CO to Pt sites can be described by accounting for the interaction of the adsorbate valence orbital with the sp orbital and d states of the adsorption site. The interaction with the sp states which are broad bands, occurs shift and band broadening of adsorbate valence band. All the transition metal especially Au and Pt (d10 and d9) have a half filled s orbital, the contribution of these sp states are similar for all transition metal. However, the anti-bonding and bonding states are formed due to the d band characteristics, which are highly localized to the adsorption site, hybridize with adsorbate.

In the case of CO, d contribution to the CO chemisorptions energy over transition metal surface

$$\Delta E_d \approx -2\left[(1-f)\frac{V_\sigma^2}{|\epsilon_d-\epsilon_{5\sigma}|}+(1+f)S_\sigma V_\sigma\right]-4\left[f\frac{V_\pi^2}{|\epsilon_{2\pi^*}-\epsilon_d|}+fS_\pi V_\pi\right]$$

In the case of OH, there are two frontier molecular orbitals

$$\Delta E_d \approx -4\left[(1-f)\frac{V_\pi^2}{|\epsilon_{1\pi}-\epsilon_d|}+(1+f)S_\pi V_\pi\right]-2\left[f\frac{V_\sigma^2}{|\epsilon_d-\epsilon_{4\sigma^*}|}+fS_\sigma V_\sigma\right]$$

2 is for the spin, f is the fractional filling of the d-bands, ϵ is the position in energy of the adsorbate states. S and V are the overlap integral and coupling

matrix. The CO and OH to Pt interaction has been same trend. To directly compare the CO strength, the CO case was further explained.

Equation can be simplified by using a two-variable, first-order Taylor expansion through

$$\Delta\Delta E = \left(\frac{\partial \Delta E}{\partial \epsilon_d}\right)_{V_{ad}} \Delta\epsilon_d + \left(\frac{\partial \Delta E}{\partial V_{ad}^2}\right)_{\epsilon_d} \Delta V_{ad}^2$$

If perturbation of the local electronic structure due to core-shell is small, the change in binding energy is linear.

$$\Delta\Delta E = \kappa_1 \Delta\epsilon_d + \kappa_2 \Delta V_{ad}^2$$

$$\left(\frac{\partial \Delta E}{\partial V_{ad}^2}\right)_{V_{ad}} = -2(1-f)\frac{V_\sigma^2}{|\epsilon_d - \epsilon_{5\sigma}|^2} - 4f\frac{V_\pi^2}{|\epsilon_{2\pi^*} - \epsilon_d|^2}$$

$$\left(\frac{\partial \Delta E}{\partial V_{ad}^2}\right)_{\epsilon_d} = -2\left[(1-f)\frac{1.3^2}{|\epsilon_d - \epsilon_{5\sigma}|} - 1.3^2\alpha(1+f)\right] - 4\left[f\frac{1}{|\epsilon_{2\pi^*} - \epsilon_d|} + \alpha f\right]$$

$S = \alpha\, V and V_\sigma = 1.3\, V_\pi$

Change in the CO adsorption energy ($\Delta\Delta E$) in response to the change in the chemical environment of the Pt, is ruled by two parameter. The first term is d-band center position and second term is interatomic matrix element which

is coupling strength of valence states of adsorbate. The first term is covalent attraction due to the hybridization between adsorbate state and substrate d-states.

Shift in the d-band is determined by the change in the d-band width. The narrow d bands are a consequence of the small coupling matrix element V_{dd}between the localized d states. Band width (W_d) is proportional to the d-d interatomic matrix $V_{dd,}$ which is related to the d- coupling strength.

Band widths are related to the center of d-band. The d-band center is related to the d-d coupling matrix and the electronegativity. (α is negative values,)

$$\Delta W_d \propto \Delta \epsilon_d = \alpha \Delta \sum_j V_{dd}^{ij} + \beta \Delta \chi$$

Due to the β is almost zero, electronegativity term can be disregarded.

$$V_{dd} \propto \frac{r_{d_i}^{3/2} r_{d_j}^{3/2}}{d_{ij}^5}$$

The d-d interatomic distance is function of spatial extent of d-orbital which is inherent property and metal-metal distance. The Pt deposited to the Au surface, the Pt was affected tensile strength which increased the d-band center. The d-band center upshift to Fermi level means the increased chemisorptions energy. $d_{Au\text{-}Pt}$ is larger than that of the $d_{Pt\text{-}Pt}$. Smaller

d_{ij}induced the larger V_{dd}. larger V_{dd} are correlated to the narrow bandwidth which are related to the d-band upshift. The greater the overlap between neighbors, the greater the bandwidth.[78]

However, the second term is repulsion term which is related to the energy cost associated to the orbital othogonalization. When the electronic states of two atoms overlap, quantum mechanics dictates that they be orthogonal to each other. This drives up the energy and lead to so-called Pauli repulsion.[79] The coupling matrix V_{ad} is function of the adsorbate-metal bond distance, d and spatial extent of metal d-orbital, r_d which is inherent parameter

$$V_{ad} \propto \frac{r_d^{3/2}}{d^{7/2}}$$

The only variable term is d in case of core-shell and alloy. The bond distance of d is linear relationship with the difference of electronegativity.

$$\Delta d = \gamma\left(\left[\prod_i^N \chi_i^{mn}\right]^{\frac{1}{N}} - \chi_{Pt}\right) = \gamma\Delta\chi$$

The proportionality coefficient γ is about -0.1. It means that the sp orbital

also affects the adsorption intensity.

Conventional expression of correlation between center of d-band and OH adsorption intensity and CO chemisorptions intensity was well conducted. However, in our cases (Au/Pt), conventional expression does not satisfy with the trend. Conventional interpretation disregarded the importance of second term due to similar electronegativity. Second term should be considered simultaneously. Second term is not new theory. It has been reported that the importance of second term. B. Hammer and J. K. Norskov et al. reported that the reason of Au nobility.[79] Pt and Ni is active than the Au due to the degree of filling of the antibondingadsorbate-metal d states. In case of Cu, the size of the overlap between the interacting atoms or molecules and the fold d states of gold is large.

The linear relationship of CO chemisorptions trend may be explained with equation. In case of small deposition of Pt to Au, the tensile strength affects dominantly. CO chemisorptions energy is larger than Pt. However, the amount of Pt deposited to the Au increased, the tensile strength decreased. Up to one monolayer, the amount of charge transfer is nearly same. In the case of Au@Pt_0.65 the Pt shell thickness is over 1, the CO chemisorptions intensity is rather increased compared to Au@Pt_0.5, regardless of smaller tensile strain confirmed by HRPD Rietveld analysis. This intriguing

featureswas first verified with experimental results.

In case of the alloy AuPt nanoparticles, the overall trend which the CO chemisorptions energy decreased as increasing the amount of Pt deposition. However, compared to the core-shell structure, the CO chemisorptions strength are even larger than alloy cases in the region of surface Pt composition > 70%. Even though the same Pt surface composition, the bulk ratio of Pt to Au is larger in case of the alloy samples. Due to the large amount of Pt, the extent of tensile strength may be smaller than that of the core-shell cases. However, from the strain term, the low chemisorptions energy does not fully explained in theory.

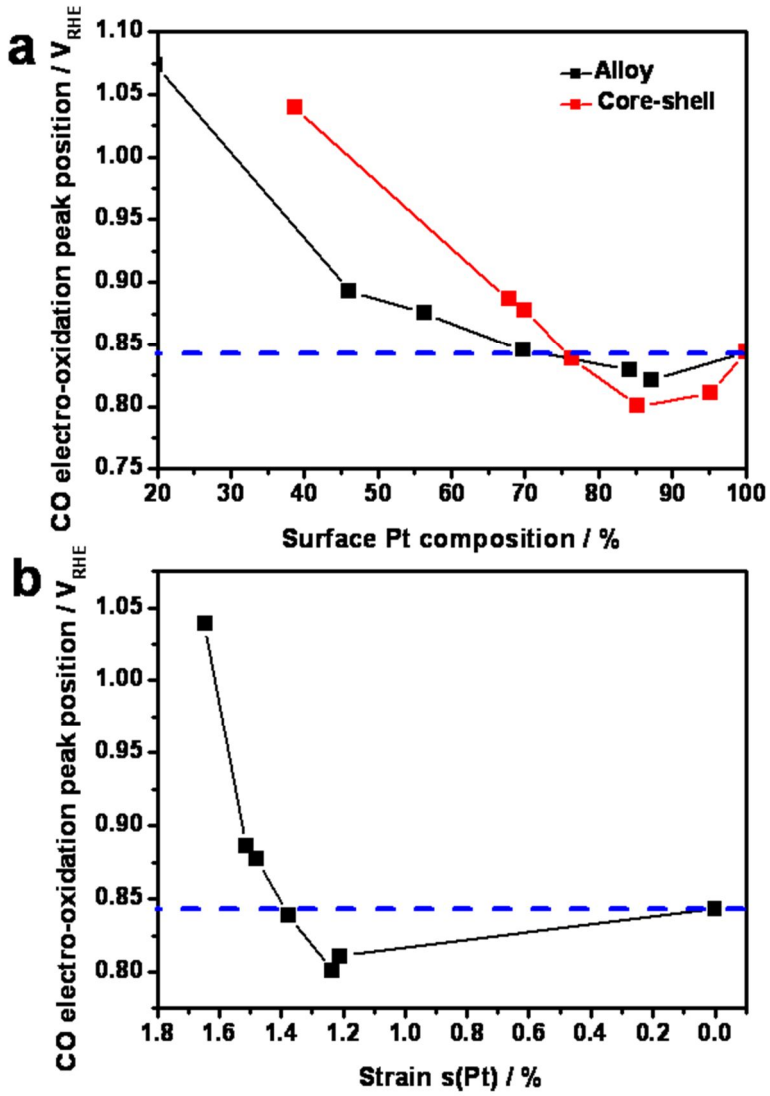

Figure 3.19.(a) CO electro-oxidation peak potential summary and (b) strain versus CO electro-oxidation peak potential

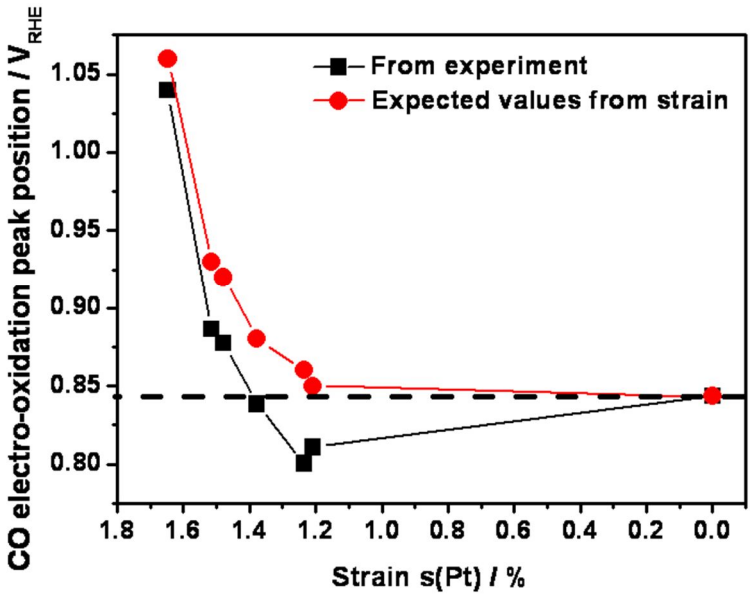

Figure 3.20. Experimental results of CO electro-oxidation and theoretical expectation values based on the d-band center model.

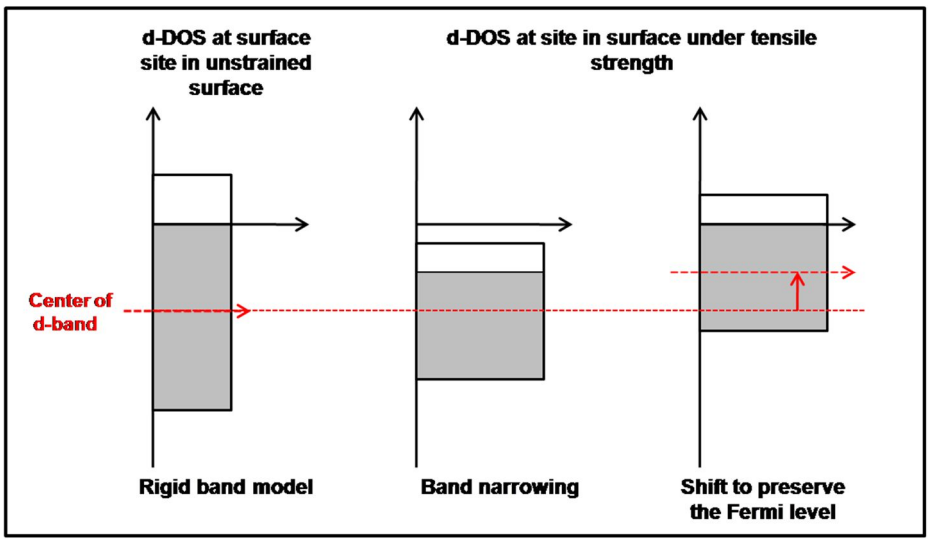

Figure 3.21. Illustration of the effect of tensile strain on the d-band center. Increasing the lattice constant shrinks the band width, to keep Fermi level, the d states have to move up in energy. (Adapted from the B. Hammer and J.K. Norskov et al., Adv. Catal., **2000**, 45,71)

The charge transfer from Pt to Au should be confirmed to explain the weak chemisorptions energy through electronic repulsion term and controversy between core-shell and alloy nanoparticles. The X-ray absorption Near Edge Structure (XANES) is very powerful techniques to quantify the hole population which are cross–related to the electron population. To confirm the Pt electron density, Pt L_3 edge was measured. Due to the proximity of Au L_3 edge, the normalization should be carefully conducted. After the normalization, the composition between Pt to Au easily confirmed which are very closed to the ICP analysis results. The L_3 edge is transition from Pr $2p_{3/2}$ to $5d_{5/2}$ and $5d_{3/2}$. If the charge transfer from Pt to Au occurs, the XANES white line intensity should be decreased. The XANES L_3 edge white line intensity directly shows the emptiness of metal d-band. However the p population also be included due to the orbital hybridization. The whiteline intensity of Au@Pt decreased compared to the Pt. White line intensity is affected by the many factors such as particle size and coordination number. Due to the complexities, the trend of XANES spectra within Au@Pt is not clearly shown. However all the white line intensity is higher than that of the Pt. The most intriguing factors are the case of alloy AuPt cases. The whiteline intensity of AuPt nanoparticles was lower than that of the Pt except for Au1Pt0.5 particles. The direction of charge transfer is opposite. Recently,

Teng. X. et al. reported that the direction of charge transfer in Au/Pt system.[60, 80] In the case of phase separated system such as core-shell structure, charge redistribution of core-shell with complete Au and Pt segregation, finding d charge depletion at the Pt site and d-charge gain at Au site. Charge redistribution can be attributed to the difference of electronegativity of local structure. However, in the case of mixed phases such as alloy structures, alloying between Au and Pt drives the system toward the covalent limit, where the d bandwidth is much larger than the energy separation of the d bands, forcing Pt and Au toward equal electron counts in the alloy system. Our XANES results werewell matched with these reports. Due to the different direction of charge transfer, the CO chemisorption tendency differed. In the case of alloy nanoparticles, their electron transfer from Pt to Au is not favorable for the second term. This reason can induce the relatively higher chemisorptions energy even though the low tensile strength. From the analysis, the alloy structure may not be good for the CO electro-oxidation reaction and also ORR activity.

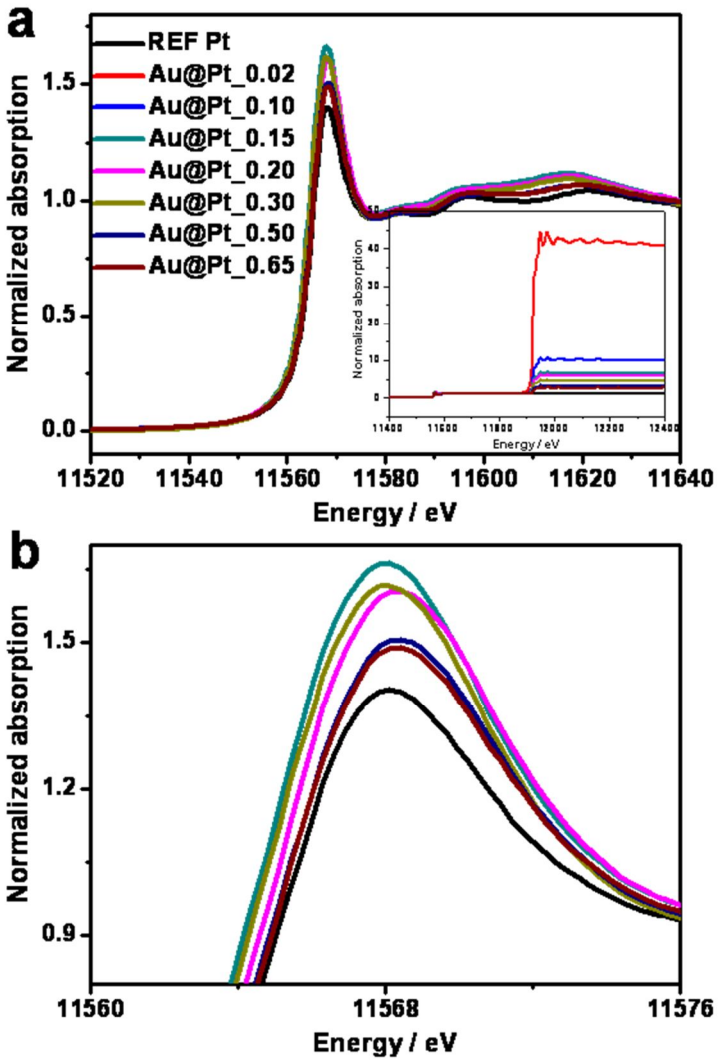

Figure 3.22. Pt L3 XANES results of Au@Pt nanoparticles

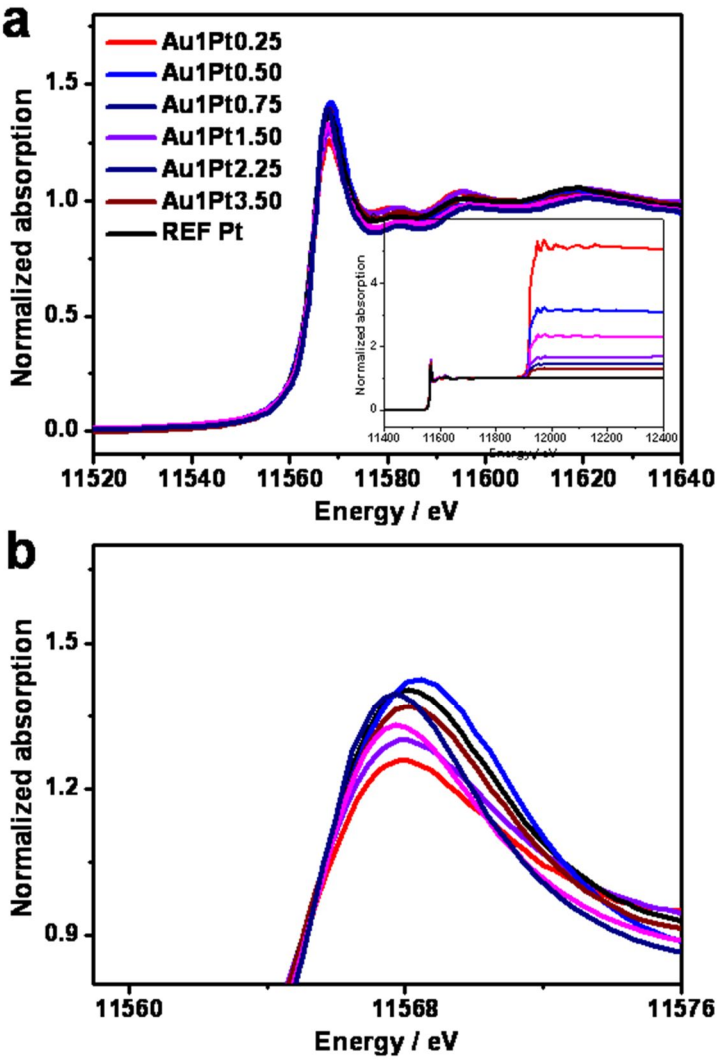

Figure 3.23. Pt L3 XANES results of AuPt alloy nanoparticles

The charge transfer of Pt to Au was also confirmed in X-ray photoemission spectroscopy (XPS). By increasing the amount of Pt deposition, the peak shifted to the high electron energy. By fixing the each energy of Pt oxidation states to compare the oxidation states, the fitting results clearly showed the decrease of Pt (0) states. However, all the Au@Pt samples had lower Pt (0) states compared to the Pt which means the charge transfer from Pt to Au.[81] In the case of the alloy nanoparticles, the amount of Pt decreased, the binding energy of Pt 4f shifted to the lower binding energy which was well agreed with previous results.[82] Low binding energy was related to the two explanations. The charge transfer from Au to Pt is the first possibility. As discussed earlier, even though the electronegativity of Pt is smaller than that of the Au, the electron transfers from Au to Pt due to the Fermi-level. The other possibility is the valence band shift induced the core level shift. J. Rodriquez and D. W Goodman et al., the valence band shift induced the core-level shift.[83] Due to the electronic change, the Pt d-band may up-shifted which is related to the strain effect and also well matched with our experimental results. The opposite electron transfer also be confirmed in XPS results again.

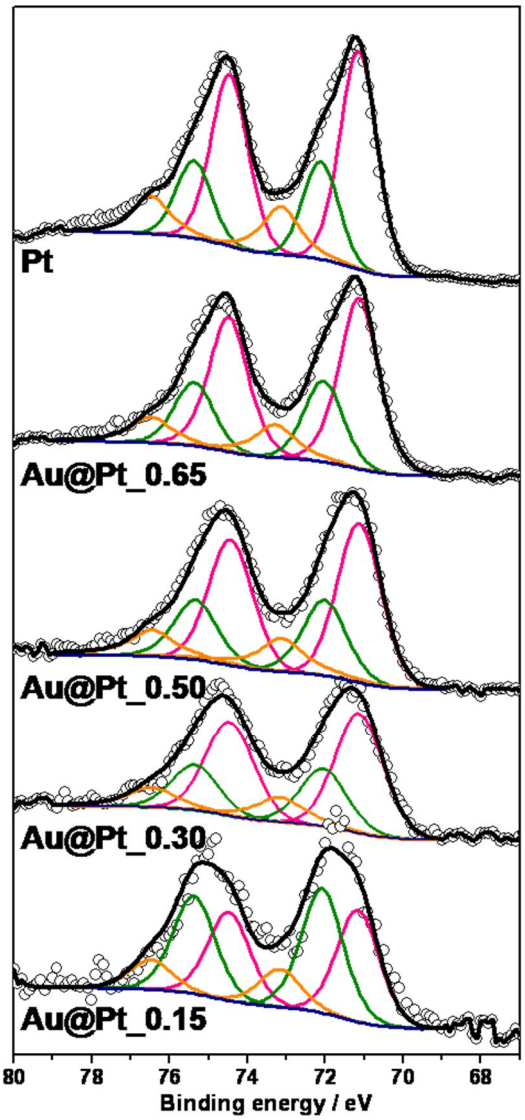

Figure 3.24. Pt 4f XPS results ofAu@Pt nanoparticles

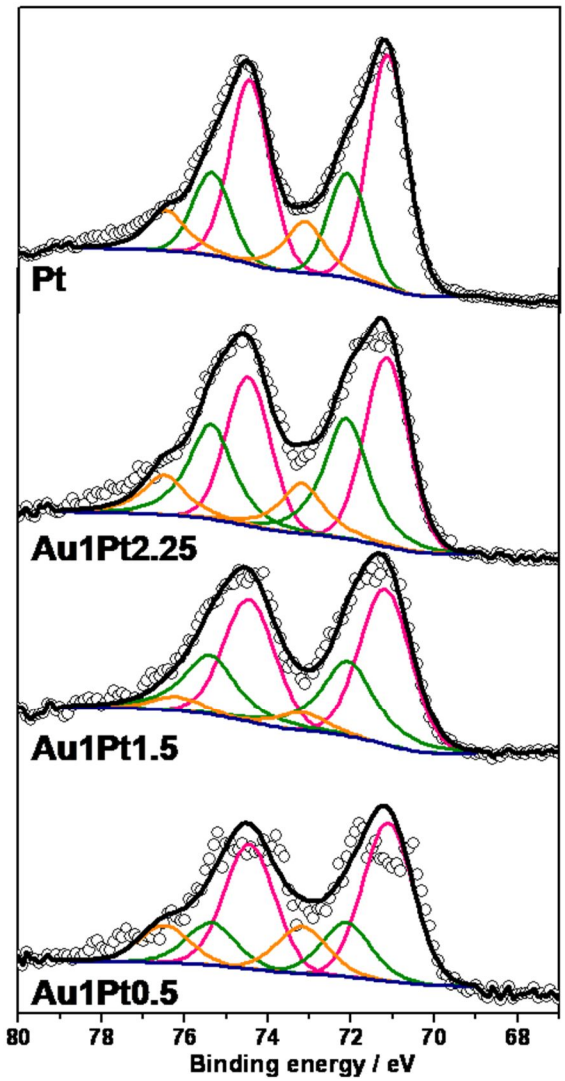

Figure 3.25. Pt 4f XPS results ofAuPt alloy nanoparticles

3.1.4. Oxygen reduction reactions

After scanning of the strength energy between Pt-CO, the Oxygen Reduction Reaction (ORR) was measured. The ORR activity was measured using rotating disk electrode under 0.1 M $HClO_4$ at 20^{o}C. The geometrically normalized activity, which means normalized with area of glassic carbon, the activity trend of core shell nanoparticles was as followed, Au@Pt_0.65 > Pt~ Au@Pt_0.50 > Au@Pt_0.30 > Au@Pt_0.20 > Au@Pt_0.15 > Au@Pt_0.10. In the case of alloy nanoparticles, the activity trend followed as Pt > Au1Pt3.5 > Au1Pt2.25 > Au1Pt1.5 > Au1Pt0.75 > Au1Pt0.5 > Au1Pt0.25. The general trend of alloy and core-shell is which the activity enhanced as increased Pt amount. The half wave potential which is the voltage at the half of limiting current, trend also showed the activity trend directly.

The specific activity normalized by Pt area results was as followed as shown in Figures. Interestingly, the specific activity trend of core-shell structure and alloy structure is similar to the CO stripping results. The CO chemisorptions strength is directly correlated with the ORR activity. As discussed earlier, the trend of CO chemisorptions energy and Pt-OH strength is same trend. The specific activity of Au@Pt_0.5 is 1.5 times higher than that of the Pt. This results shows that the composition dependent ORR activity was governed by the strength of oxygen species. Due to the weak chemisorptions energy, the

surface free sites ($1-\theta_{ad}$) increased in the case of Au@Pt_0.5.

Our suggested model for elucidating unprecedented features on the CO chemisorptions strength and ORR activity may well suited. This model may be explained the unknown reason for deviation between experimental results and the theoretical calculation in Cu case. The activity trend of Pt modified Cu system. Experimental data shows that the optimum composition of Pt/Cu is deviated to the theoretical calculation which is based on the d-band center model. The low current compared to the theoretical configuration may stems from the second term which are the electronic repulsion term.[84]

In the case of Cu, the electronegativity of Cu is smaller than that of the Pt. The charge transfer from Cu to Pt may induce the bond length between adosrbate such as OH and CO to Pt. Due to the short bond length, the orbital overlap affects the chemisorptions energy.

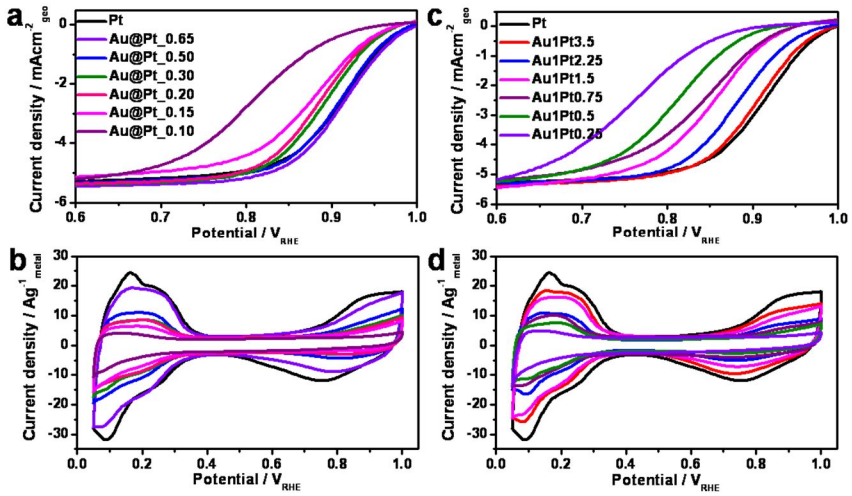

Figure 3.26.ORR results andcyclic voltammograms of (a-b) Au@Pt nanoparticles and (c-d) in the case of AuPt alloy nanoparticles

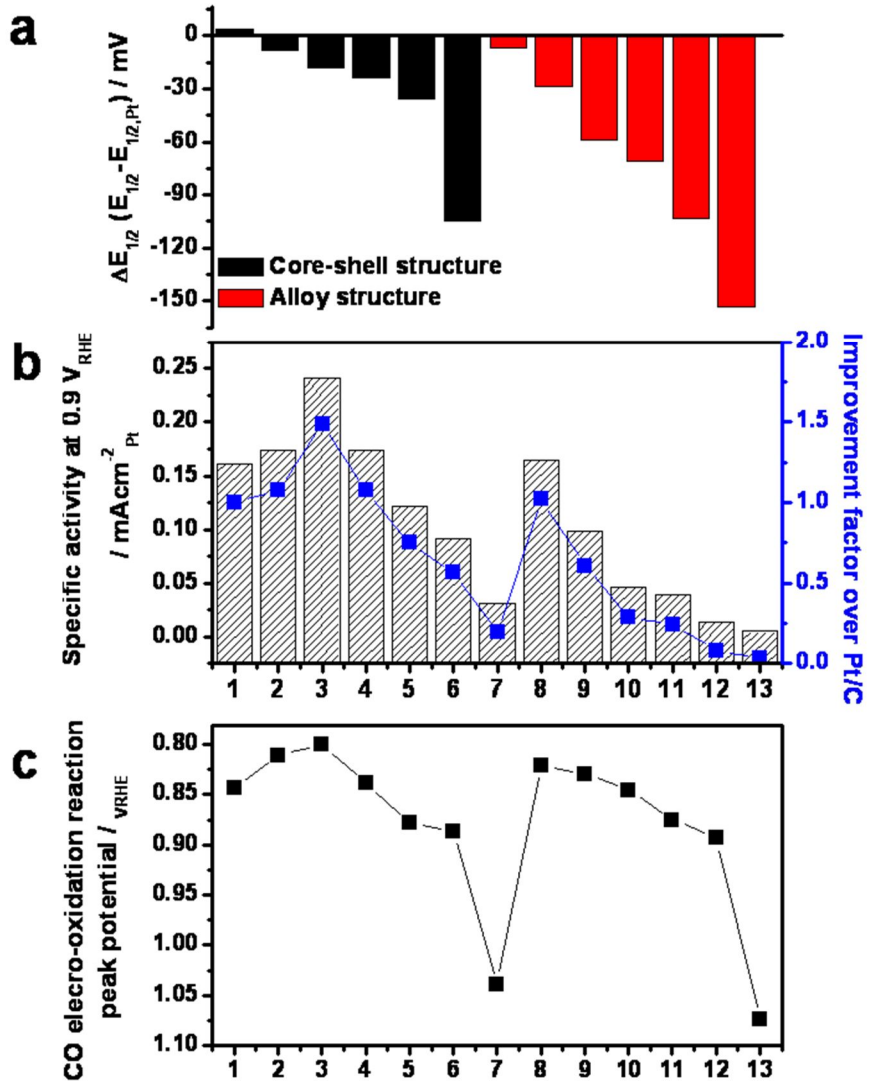

Figure 3.27.(a) Half wave potential, (b) specific activity at 0.9V, and (c) CO stripping results summary

3.2. How to improve the ORR activity in Au/Pt systems?

3.2.1. Difference between single crystal and nanoparticles

The most intriguing results could be summarized as two parts. The first is Au@Pt system can be a good model for the designing the electrocatalysts for fuel cells. Especially, the orbital repulsion terms should be considered when the electronegativity difference may not be disregarded in the local environments. Due to the orbital repulsion parameter, the chemisorptions energy of OH and CO can lower compared to Pt. The second term is why the Au@Pt has lower activity compared to Pt in single crystal model cases. In other words, the activity enhancement of Au@Pt occurred in nanoscale only. The reason of this part is very important for designing the "nanoscale" electrocatalyst.

From the equation which is governed by the quantum chemistry, the two parameters affect the chemisorption energy. The second term may not be changed in nanoscale. The only possible term is the key parameter in scale difference. In the case of nanoparticle, the surface strain effects have been reported. The driving force for this contraction has been attributed to the smoothing of surface electron density and a resulting electrostatic force that pulls the surface ions towards the bulk or to a change in chemical bond where the lowered coordination numbers strengthen the remaining

bond.[85]The Smoluchowski smoothing effect is a distribution of the electron cloud on a metal surface with a strong corrugation.[86] A higher gradient in the charge density leads to a higher kinetic energy. To lower the kinetic energy, the charge distribution is smoothed out. Considering the nanoparticles, there are lots of low coordinated sites in surface. W.J. Huang et al. reported that the coordination-dependent surface atomic contraction in nanocrystals by coherent diffraction.[87] From the results, the average atomic bond lengths at the surface are found to reduce by 1-8%. The amount of contraction increase with decreasing the coordination numbers in the model and experimental results, simultaneously. Interestingly, the bond length variation through the coordination number change was around 10 %. In 2D (111) single crystal cases, the coordination numbers of surface atoms are about 9 considering the broken bond model. However, in the case of nanoparticles, their surface coordination number may be much lower than that of the single crystal. The discrepancy between single crystal study and nanoparticle case may stems from the coordination dependent strain effect. The Au@Pt nanoparticle, the shell materials, Pt, has little affected by the Au tensile strength compared to bulk model. The Au surface was contracted in nanoparticles which are about 3 nm size which induced the low degree of tensile strength. Relatively low effect of tensile strength, the electronic

repulsion term can be dominant parameter in some compositions, which is directly related to the strain effect.

3.2.2. Surface coordination number control and strain effects

To confirm the effect of coordination-dependent strain effect, the coordination changed in similar size. The coordination number is dependent on the size of nanoparticles. By varying the size of nanoparticles, the coordination number can be tuned easily. However, the size of nanoparticle also affects the nature of materials significantly in nanoscale due to the quantum confinement effects. The most serious problems with size variation are size dependent electrochemical activity. The size dependent of ORR activity has been studied for a long times. The exact correlation was under consideration, however the size dependent activity change was confirmed. Without significant size variation, coordination number control is important. The sonochemical method is the possible method to control the coordination number in Au nanoparticles.[88] It was reported that the high temperature conditions produce a large number of coordinatively unsaturated which is low coordination Au atoms on the surfaces. Due to the high density of low coordination number, the hydrogen oxidation reaction activity enhancement was confirmed. Direct heating may be impossible in nanoparticle due to the

agglomeration and sintering. The sonication is short time induced heating with a decay rate of 1010K s-1.[89][90]The supercooled molten states of Au nanoparticles have been made without substantial particle size change. From the molecular dynamics and experiment results, the coordination numbers of Au nanoparticles can be tuned. As prepared Au/C (30 wt.%) nanoparticle was dissolved in ethanol and ultrasonicated in 1 hr. The difference between the unmodified Au/C and sonochemical method treated Au/C was not confirmed in conventional TEM analysis. The XRD results were also not changed. Investigating the coordination number change was conducted by EXAFS analysis. The Au L_3 edge was measured. After fitting process with ATHENA and ARTEMIS, the following results were summarized in Table. Interestingly, the coordination number of Au_S nanoparticles decreased. Considering the relatively large errors in coordination number quantitative analysis in EXAFS, however the atomic distance decrease and the increase of Deby-waller factor, the coordination number decrease was confirmed.[91, 92]

To clearly confirmation of coordination number change, hydrogen oxidation reaction was conducted. In bulk Au, there has no activity in catalysis. However, the emergence of catalytic activity of gold occurs by decreasing the size. The activity enhancement may stem from the low

coordination induced high chemisorptions energy of adsorbate. N. Lopez et al. reported that the binding energy of oxygen species with respect to the coordination number of the Au atoms of the sites. From the results, the chemisorptions energy increased by decreasing the coordination number. HOR activity was measured under the 0.1 M $HClO_4$ and H_2 saturated conditions. Before the measurements, the surface of catalyst was cleaned by cycling from the 0.05 V to 1.0 V_{RHE} under Ar condition. The HOR activity of sonochemical treated Au/C has higher than that of the unmodified Au/C. The activity enhancement may be originated from the surface coordination number tuning. From the EXAFS and HOR activity analysis, the coordination number change was confirmed.

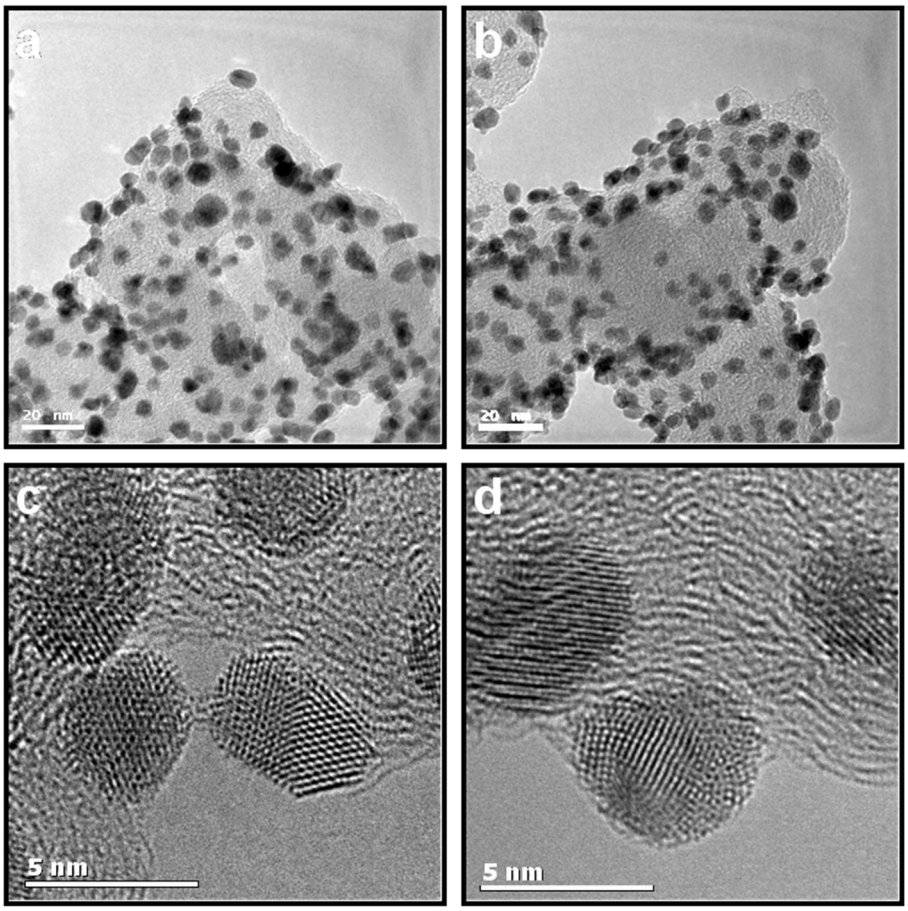

Figure 3.28.HR-TEM images of (a,c) before sonochemical methods, and (b-d) after sonochemical methods

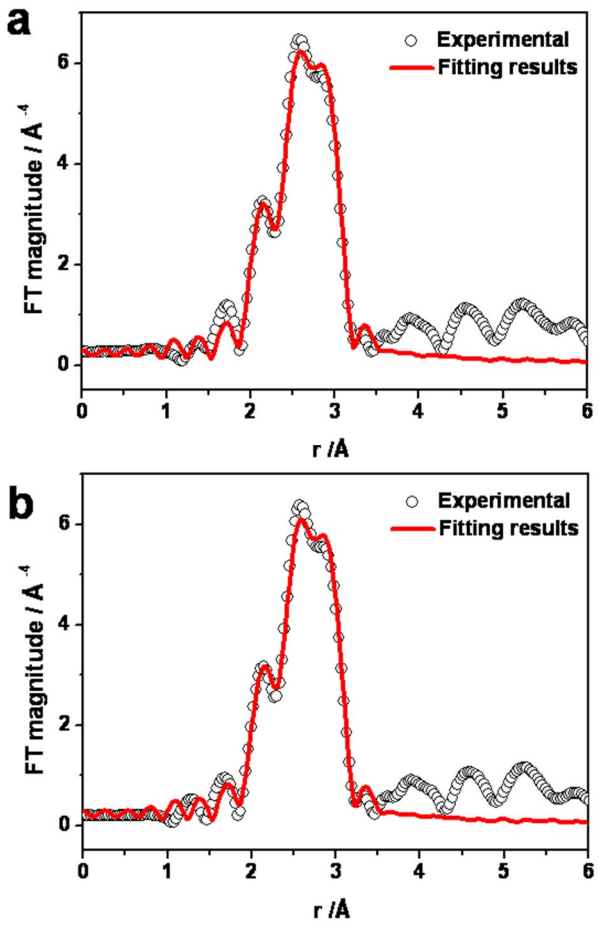

Figure 3.29. Au L3 EXAFS results of Au/C (a) before sonochemical method, and (b) after sonochemical method.

Table 3.3. Summary of Au L3 EXAFS analysis of Au/C and after sonochemical method

	Interatomic distance / Å	Coordination number / N	Debye-waller factor /Å^2	R-factor
Au	2.8505(1)	10.1(2)	0.0085	0.0053
Au_S	2.8496(7)	9.9(7)	0.0092	0.0057

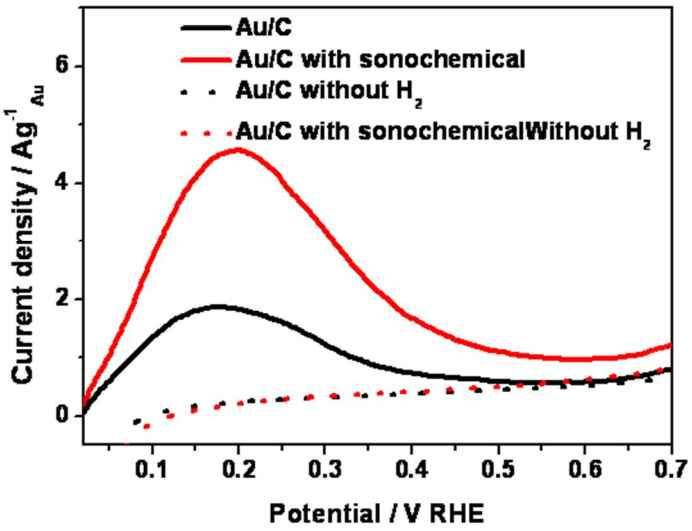

Figure 3.30. Hydrogen oxidation activity of before sonochemical method, and after sonochemical method.

To compare the effects of coordination dependent strain effect, Pt deposited to the Au/C and Au/C_S with same procedure. After the Pt deposition, the synchrotron HRPD analysis was conducted to confirm the strain effect. The analysis was conducted two step method. As synthesized Au/C and sonochemical treated Au/C HRPD was refined by Rietveld analysis. Using the refined parameter, the Au@Pt_0.5 and Au@Pt_0.5_S was refined with fixed Au core parameter. Even though the lattice also changed by Pt deposition, due to the pseudomorphic layer deposition, this effect may be confined with little amount and also included in the Pt lattice parameter. The Pt lattice parameter from the Rietveld analysis of Au@Pt_0.5_S decreased about 0.015 Å. From the strain calculation compared bulk Pt, the strain of Au@Pt_0.5 was about 1.23 and the case of Au@Pt_S was about 0.83 which is 0.4 % lower than unmodified ones. The Pt deposition on the low coordinated core Au atoms had smaller lattice parameter.

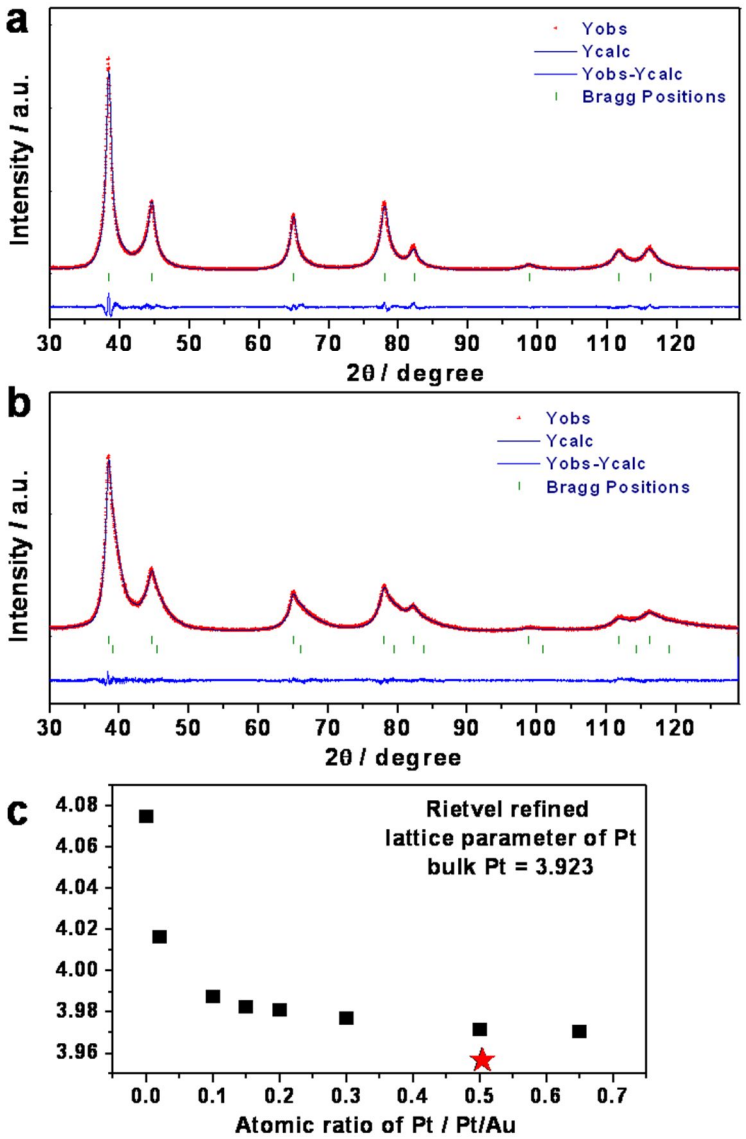

Figure 3.31.HRPD results of (a) Au/C with sonochemical method, (b) Au@Pt_0.5_S and (c) Rietveld refinement results.

Table 3.4. Summary of HRPD Rietveld refinement analysis

Sample	Lattice parameter of Au	Lattice parameter of Pt	R_p	R_{exp}	R_{wp}	S
Au	4.07510(1)	-	2.99	3.48	5.22	1.5
Au_S	4.07341(7)	-	3.12	3.51	5.62	1.6
Au@Pt_0.5	4.07510(1)*	3.97151(6)	5.11	3.39	5.09	1.5
Au@Pt_0.5_S	4.07341(7)*	3.96261(9)	3.20	3.60	4.32	1.2

R_p : Profile factor, R_{exp} : expected weighted profile factor,
Rwp : weighted profile factor, S : goodness of fit indicator

The ORR activity was measured Au@Pt_0.5_S samples. The ORR activity of Au@Pt_0.5 was relatively same with the Pt/C nanoparticles. The ORR activity of Au@Pt_0.5_S nanoparticles was superior ORR activity compared with Pt/C and Au@Pt_0.5. The half wave potential was positively shifted 20 mV. The specific current density with normalized Pt area was 2.5 times higher compared to Pt/C and 1.8 times higher than Au@Pt_0.5. This activity enhancement may be related to the low strain effect by low coordination number induced, and the orbital repulsion effect.

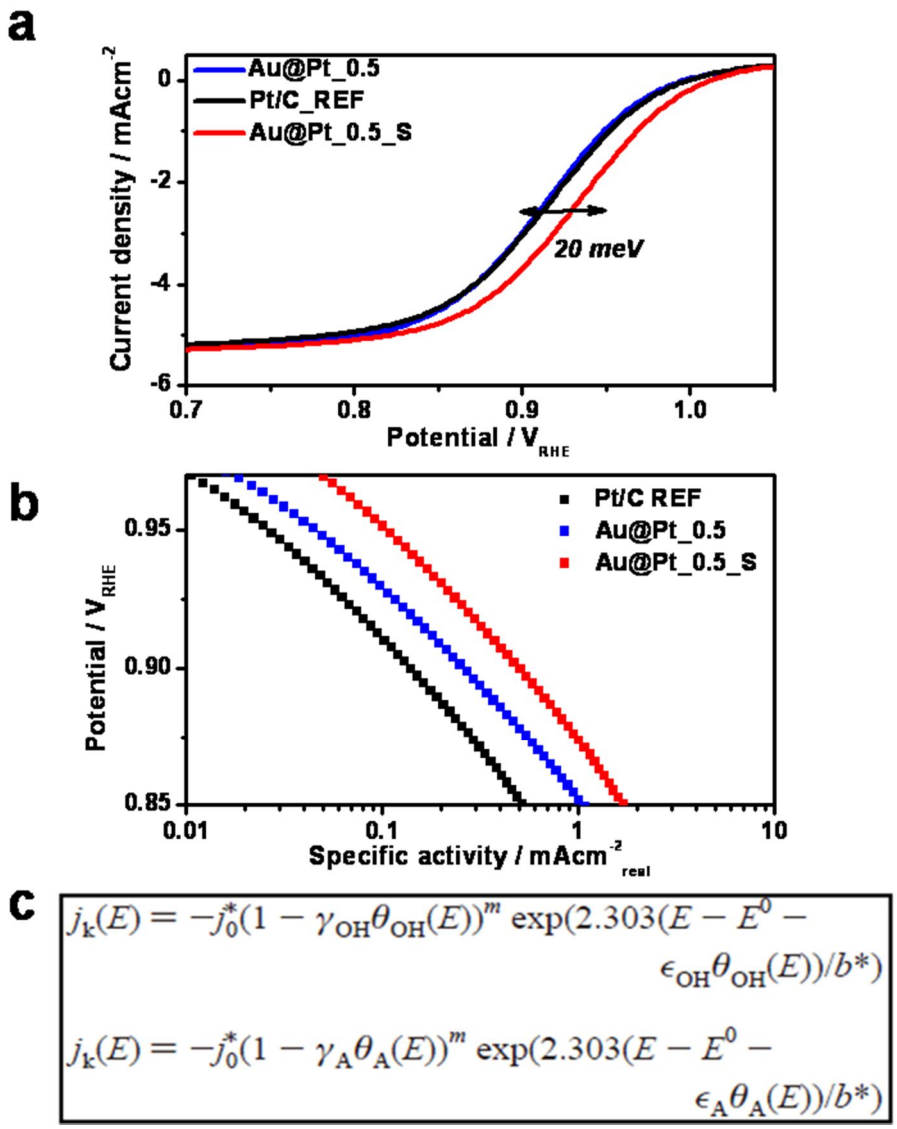

Figure 3.32.(a)ORR results of Au@Pt0.5 and Au@Pt_0.5_S and (b) Tafel plots, and (c) ORR activity theory.

Table 3.5.ORR benchmarks with the core-shell like structure and other architectures

Catalyst	Synthetic method	Specific acitivity ($mAcm^{-2}$ Pt at 0.9 V)	Mass activity/(Pt/C) (at 0.9 V)	Reference
Pt monolayer on 4.0 nm Pd/C	Cu UPD mediated electrodeposition	500 ($10mVs^{-1}$)	6	J. Am. Chem. Soc., 131,2009,17298
Pt monolayer on 4.6 nm Pd3Co/C	Cu UPD mediated electrodeposition	800 ($10mVs^{-1}$)	9.8	J. Am. Chem. Soc., 131,2009,17298
Pt monolayer porous Pd-Cu alloys/C	Cu UPD mediated for Pt deposition Electrochemical dealloying	1000-1200	2.8	J. Am. Chem. Soc., 132,2010,9253
Au/Pt/C	Cu UPD method for Au deposition on Pt/C	564 (at 0.85 V)	~1.2	Science, 315, 2007, 220
Dealloyed $Pt_{25}Co_{75}$/C	Electrochemical dealloying	491	2.2	J. Power. Sources, 196,2011,666
Dealloyed $Pt_{20}Ni_{60}Cu_{20}$/C	Electrochemical dealloying	406	3.0	J. Power. Sources, 196,2011,666
Dealloyed $Pt_{25}Cu_{75}$/C	Voltammetric surface dealloying and annealed at 800 0C for 7h	756	3.4	J. Am. Chem. Soc., 129,2007,12624
Pt on Pd bimetallic hetero-nanostructures /C	Sequential deposition	307	-	J. Am. Chem. Soc., 131,2009,7542
Truncated Octahedral Pt_3Ni/C	Colloid method	850	3.3	
Pd-Pt nanodendrites	Pd nanocrystal seeds method with L –acorbic acid as a reductant	420	1.5	Science, 324, 2009, 1302
Mesostructured Pt3Ni NSTF		~2400 (at 0.95 V)	-	Nat. Mater.,11, 2012, 1051
Pt skin of PtNi/C	Acid treat and annealed	820 (at 0.95 V)	~6.0	J. Am. Chem. Soc., 133,2011,14396
Pt on AuCu/C	Colloid method	-	2.1	Energy. Environ. Sci.,5,2012,8976
Pt segregated PtAu/C	CO heat-treatment	170	-	Appl. Catal. B, 129, 2013, 375
46 % Pt/C (TKK)		210	1	Appl. Catal. B, 56, 2009, 9
Au@Pt_0.5_S	Sequential deposition using HQ	463	4.4	

To confirm the reason of ORR activity enhancement, the CO electro-oxidation measurements was conducted. The peak potential of Au@Pt_0.5_S was negatively shifted compared to the Au@Pt_0.5, which was the most negatively shifted in various compositions. Interestingly, the peak shapes was extensively shifted to the low potential region with asymmetric. These low CO stripping peak was originated from the decrease of strain terms.

The formic acid oxidation also conducted. The electro-oxidation of formic acid activity was as follows, Au@Pt_0.5 > Pt ~ Au@Pt_0.5_S. The interaction of the Pt overlayer with the Au core plays an important role. Pt overlayer on Au generates the tensile strain due to smaller size of Pt compared to that of Au. In the case of Au@_Pt_0.5_S, the tensile strength was weakened compared to the Au@Pt_0.5. From the formic acid electro-oxidation reaction, strain control was also confirmed again.[93]

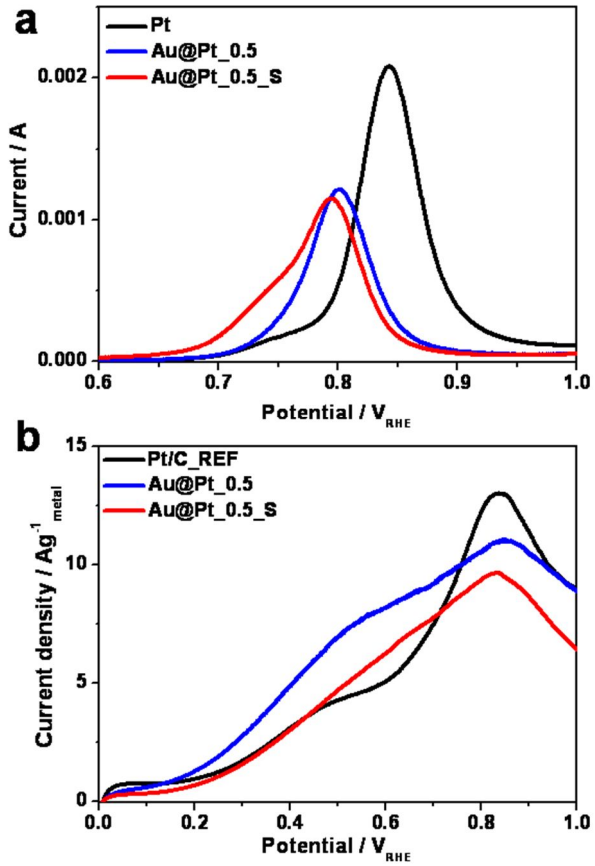

Figure 3.33. Comparisons of reaction of (a) CO electro-oxidation, (b) formic acid oxidation under H_2SO_4.

Finally the long term stability test was conducted. In DOE protocol, the ADT test was conducted potential cycling from 0.6 V to 1.0 VRHE with 50 mVs^{-1} at 20 ^{o}C 10,000 cycles.After 10,000 cycles, the ORR activity of Pt/C was decreased remarkably. However, in the case of Au@Pt_0.5_S, the activity was little deactivated compared to the initial measurement which was superior for long-term stability. From the CV, the electrochemical surface area also showed the trend. Electrochemical surface area of Pt/C decreased about ~ %, however only ~% decreased in the case of Au@Pt_0.5_S. The superior long-term stability of Au modified Pt was reported first time at R. R. Adzic group[2]. By simply adsorption of Au cluster near Pt enhance the durability up to 30,000 cycles. In-situ XANES measurements showed the decreased oxidation states by changing the potential compared to the Pt/C. The clear reason of enhanced durability was not revealed. However, many papers also have been reported enhanced durability.W. Chao et al., reported that the core (Au) – shell (PtFe) nanoparticles was also superior for ORR activity and durability.[28]The possible reason for enhanced durability was suggested as Au atoms tend to segregate to the surface due to surface free energy concerns. However, under the electrochemical conditions ($HClO_4$, 0.6 V_{RHE}< Potential < 1.0V_{RHE}), oxygen species such as OH and O are strongly bind to the Pt surface. These

controversies drive the Pt stays at the surface position. The other possible mechanism is stabilization of surface Pt due to the hindered place exchange mechanism. Au can not be oxidized at given potential. Au in the subsurface hindered the formation of surface oxide and hence suppressed the dissolution of Pt surface atoms.[28]

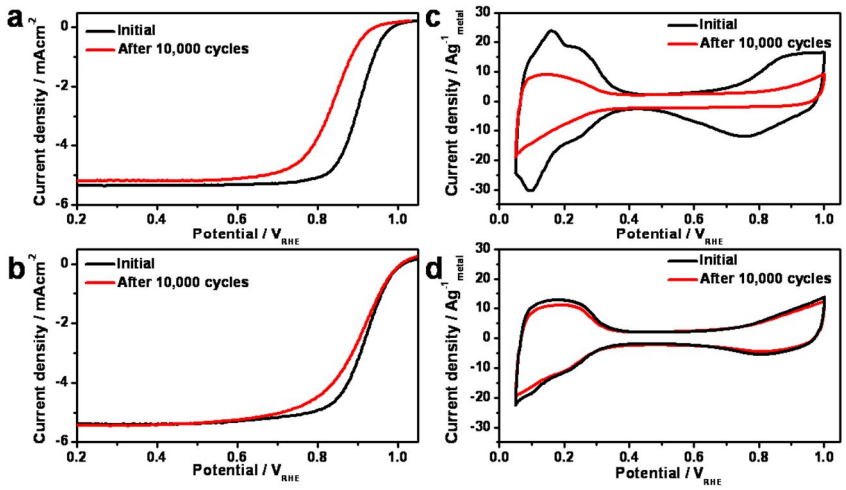

Figure 3.34. Long term durability test of (a,c) Pt/C and (b,d) Au@Pt_0.5_S

In summary, the major discern between nanoparticle and single crystal study of Au@Pt core-shell structure may be originated from the coordination dependent strain effect. In the case of nanoparticles, the bond length between atoms is lower than bulk due to the coordination induced contraction. The Au@Pt structure was regarded not ideal cases for oxygen reduction reaction by DFT calculation due to the tensile strength. However, by tuning the coordination number of surface atom, the strain effect could be smaller than the orbital repulsion term. High performance Au@Pt_0.5_S structure was designed and confirmed high ORR activity and low chemisorptionsenergy with CO molecules. Both superior ORR activity and durability could be realized by nanoscaledesigning and detail investigation.

Chapter 4.Conclusions

In this study, the Pt/Au nanoparticle systems were applied to the ORR electrocatalyst beyond the previous unfavorable expectation and single crystal studies. The Au@Pt core-shell nanosized electrocatalysts and AuPt alloy nanoparticles were synthesized. Delicate investigations of nanoparticle structure were conducted using high resolution transmission electron microscopy and x-ray diffraction. X-ray absorption fine structures and photo emission spectroscopy also conducted at synchrotron facilities to confirm the inter-atomic distances, information related to the coordination numbers and electronic structures. From the CO stripping experiments, Pt-CO chemisorptions energy was larger than that of the pure Pt until certain Pt surface compositions. However, the deposition of Pt increased, the Pt-CO chemisorptions energy is lower than pure Pt which was controversy to previous predictions which the Au induced tensile strain to Pt with high chemisorptions energy to CO and oxygen related species. To explain the experimental results, elucidations with quantum mechanics were performed. The chemisorptions energy between metal and CO and oxygen species was interpreted two terms; center of d-band structures and orbital repulsion terms. The center of d-band positions was related to the band width. By changing the local environment, the d-band structure was changed due to the changing

the orbital overlap between near atoms. Orbital repulsion terms were related to the adsorbate– metal orbital coupling matrix. The shorter the bond induced the more orbital overlap, the adsorbate anti-bonding orbital filled with the interaction between metal sp orbitals. Due to the different electronegativity between Au and Pt, orbital repulsion should also be considered. Au has higher electronegativity compared to the Pt, induced the charge redistribution from Pt to Au. The lower electron in Pt induced the shorter bond distance with adsorbate, made the repulsion. The two parameters were mixed in Au/Pt systems. In the case of low Pt deposition to surface, the strain induced d-band center overwhelmed the effect of orbital repulsion terms. As amount of surface Pt increased, the strain factors decreased. Orbital repulsion factors were no longer the minor parameter at certain points. In the case of AuPt alloy nanoparticles, their flow of electron redistribution was different to core-shell structures. Considering the electronic structures, the core-shell structures were good candidates for ORR electrocatalysts. The ORR activity trends also followed with the CO stripping results.

The different results between previous single crystal studies and current nanoparticle case were explained with the characteristics of nanoparticles. In the case of nanoparticles, their surface atoms have low coordinated which

induces the surface atom contraction. Due to the surface contraction effect, the tensile strength was little effects on the Au@Pt system in nanoparticles. To confirm the nanosized atomic contraction effects, the surface coordination number was controlled using sonochemical method. The coordination number control was confirmed using extended x-ray absorption fine structures. The fitting parameter was shown as low coordination number, smaller inter-atomic distances and high Debye waller factors. Hydrogen oxidation reaction was also confirmed the surface low coordination number after sononchemicalmethods. After the coordination number controls, the Pt deposited to the Au nanoparticles. The lattice parameter of Pt was investigated using Rietveld refinement. The Pt deposited with low coordination numbered Au had low lattice parameter. Controlling the surface coordination number of core nanoparticle, strain could be controlled. The Au@Pt_0.5_S had 1.7 times higher ORR activity compared to without sononchemical method and 2.5 times higher activity compared to Pt nanoparticles.

From these researches, the possible factors related to the adsorbate chemisorption energy were considered; center of d-band structures and orbital repulsion under the quantum mechanics. The strain effects could be controlled with change of coordination number of nanoparticles. These

considerations can be applied to the strategies to design the "nanoscale"electrocatalysts.

References

[1] H.A. Gasteiger, N.M. Markovic, Just a dream or future reality?, Science, **2009**, 324, 48-49.

[2] J. Zhang, K. Sasaki, E. Sutter, R.R. Adzic, Stabilization of platinum oxygen-reduction electrocatalysts using gold clusters, Science, **2007**, 315, 220-222.

[3] V. Mazumder, Y. Lee, S. Sun, Recent development of active nanoparticle catalysts for fuel cell reactions, Adv. Funct. Mater., **2010**, 20, 1224-1231.

[4] J.K. Nørskov, J. Rossmeisl, A. Logadottir, L. Lindqvist, J.R. Kitchin, T. Bligaard, H. Jónsson, Origin of the overpotential for oxygen reduction at a fuel-cell cathode, J. Phys. Chem. B, **2004**, 108, 17886-17892.

[5] N.M. Marković, H.A. Gasteiger, P.N. Ross Jr, Oxygen reduction on platinum low-index single-crystal surfaces in alkaline solution: Rotating ring diskPt(hkl) studies, J. Phys. Chem., **1996**, 100, 6715-6721.

[6] J. Greeley, I.E.L. Stephens, A.S. Bondarenko, T.P. Johansson, H.A. Hansen, T.F. Jaramillo, J. Rossmeisl, I. Chorkendorff, J.K. Nørskov, Alloys of platinum and early transition metals as oxygen reduction electrocatalysts, Nat. Chem., **2009**, 1, 552-556.

[7] T. Bligaard, J.K. Nørskov, S. Dahl, J. Matthiesen, C.H. Christensen, J. Sehested, The Brønsted-Evans-Polanyi relation and the volcano curve in heterogeneous catalysis, J. Catal., **2004**, 224, 206-217.

[8] J.L. Fernández, D.A. Walsh, A.J. Bard, Thermodynamic guidelines for

the design of bimetallic catalysts for oxygen electroreduction and rapid screening by scanning electrochemical microscopy. M-Co (M: Pd, Ag, Au), J. Am. Chem. Soc., **2005**, 127, 357-365.

[9] T. Toda, H. Igarashi, H. Uchida, M. Watanabe, Enhancement of the electroreduction of oxygen on Pt alloys with Fe, Ni, and Co, J. Electrochem. Soc., **1999**, 146, 3750-3756.

[10] S. Mukerjee, S. Srinivasan, M.P. Soriaga, Role of structural and electronic properties of Pt and Pt alloys on electrocatalysis of oxygen reduction, J. Electrochem. Soc., **1995**, 142, 1409-1422.

[11] S. Mukerjee, S. Srinivasan, Enhanced electrocatalysis of oxygen reduction on platinum alloys in proton exchange membrane fuel cells, J. Electroanal. Chem., **1993**, 357, 201-224.

[12] G.F. Wei, Z.P. Liu, Optimum nanoparticles for electrocatalytic oxygen reduction: The size, shape and new design, PCCP, **2013**, 15, 18555-18561.

[13] A. Ruban, B. Hammer, P. Stoltze, H.L. Skriver, J.K. Nørskov, Surface electronic structure and reactivity of transition and noble metals, J. Mol. Catal. A: Chem., **1997**, 115, 421-429.

[14] J.K. Nørskov, T. Bligaard, A. Logadottir, S. Bahn, L.B. Hansen, M. Bollinger, H. Bengaard, B. Hammer, Z. Sljivancanin, M. Mavrikakis, Y. Xu, S. Dahl, C.J.H. Jacobsen, Universality in heterogeneous catalysis, J. Catal., **2002**, 209, 275-278.

[15] J.K. Nørskov, T. Bligaard, B. Hvolbæk, F. Abild-Pedersen, I. Chorkendorff, C.H. Christensen, The nature of the active site in

heterogeneous metal catalysis, Chem. Soc. Rev., **2008**, 37, 2163-2171.

[16] L. Gan, M. Heggen, R. O'Malley, B. Theobald, P. Strasser, Understanding and controlling nanoporosity formation for improving the stability of bimetallic fuel cell catalysts, Nano Lett., **2013**, 13, 1131-1138.

[17] D.A. Slanac, A. Lie, J.A. Paulson, K.J. Stevenson, K.P. Johnston, Bifunctional catalysts for alkaline oxygen reduction reaction via promotion of ligand and ensemble effects at Ag/MnO x nanodomains, J. Phys. Chem. C, **2012**, 116, 11032-11039.

[18] D. Friebel, V. Viswanathan, D.J. Miller, T. Anniyev, H. Ogasawara, A.H. Larsen, C.P. Ogrady, J.K. Nørskov, A. Nilsson, Balance of nanostructure and bimetallic interactions in Pt model fuel cell catalysts: In situ XAS and DFT study, J. Am. Chem. Soc., **2012**, 134, 9664-9671.

[19] Y. Chen, Z. Liang, F. Yang, Y. Liu, S. Chen, Ni-Pt core-shell nanoparticles as oxygen reduction electrocatalysts: Effect of Pt shell coverage, J. Phys. Chem. C, **2011**, 115, 24073-24079.

[20] L. Dubau, F. Maillard, M. Chatenet, J. André, E. Rossinot, Nanoscale compositional changes and modification of the surface reactivity of Pt3Co/C nanoparticles during proton-exchange membrane fuel cell operation, Electrochim. Acta, **2010**, 56, 776-783.

[21] E.A. Lewis, C.U. Segre, E.S. Smotkin, Embedded cluster Δ-XANES modeling of adsorption processes on Pt, Electrochim. Acta, **2009**, 54, 7181-7185.

[22] M.P. Hyman, J.W. Medlin, Effects of electronic structure modifications

on the adsorption of oxygen reduction reaction intermediates on model Pt(111)-alloy surfaces, J. Phys. Chem. C, **2007**, 111, 17052-17060.

[23] J. Wu, L. Qi, H. You, A. Gross, J. Li, H. Yang, Icosahedral platinum alloy nanocrystals with enhanced electrocatalytic activities, J. Am. Chem. Soc., **2012**, 134, 11880-11883.

[24] M. Oezaslan, P. Strasser, Activity of dealloyed PtCo3 and PtCu3 nanoparticle electrocatalyst for oxygen reduction reaction in polymer electrolyte membrane fuel cell, J. Power Sources, **2011**, 196, 5240-5249.

[25] J. Yang, J.Y. Lee, Q. Zhang, W. Zhou, Z. Liu, Carbon-supported pseudo-core-shell pd-pt nanoparticles for ORR with and without methanol, J. Electrochem. Soc., **2008**, 155, B776-B781.

[26] M. Oezaslan, F. Hasché, P. Strasser, Pt-based core-shell catalyst architectures for oxygen fuel cell electrodes, Journal of Physical Chemistry Letters, **2013**, 4, 3273-3291.

[27] S.J. Hwang, S.J. Yoo, J. Shin, Y.H. Cho, J.H. Jang, E. Cho, Y.E. Sung, S.W. Nam, T.H. Lim, S.C. Lee, S.K. Kim, Supported core at shell electrocatalysts for fuel cells: Close encounter with reality, Scientific Reports, **2013**, 3.

[28] C. Wang, D. Van Der Vliet, K.L. More, N.J. Zaluzec, S. Peng, S. Sun, H. Daimon, G. Wang, J. Greeley, J. Pearson, A.P. Paulikas, G. Karapetrov, D. Strmcnik, N.M. Markovic, V.R. Stamenkovic, Multimetallic Au/FePt3 nanoparticles as highly durable electrocatalyst, Nano Lett., **2011**, 11, 919-926.

[29] P. Mani, R. Srivastava, P. Strasser, Dealloyed binary PtM3 (M = Cu, Co, Ni) and ternary PtNi 3M (M = Cu, Co, Fe, Cr) electrocatalysts for the oxygen reduction reaction: Performance in polymer electrolyte membrane fuel cells, J. Power Sources, **2011**, 196, 666-673.

[30] H. Zhang, Y. Yin, Y. Hu, C. Li, P. Wu, S. Wei, C. Cai, Pd@Pt core-shell nanostructures with controllable composition synthesized by a microwave method and their enhanced electrocatalytic activity toward oxygen reduction and methanol oxidation, J. Phys. Chem. C, **2010**, 114, 11861-11867.

[31] D. Wang, H.L. Xin, Y. Yu, H. Wang, E. Rus, D.A. Muller, H.D. Abruña, Pt-decorated PdCo@Pd/C core-shell nanoparticles with enhanced stability and electrocatalytic activity for the oxygen reduction reaction, J. Am. Chem. Soc., **2010**, 132, 17664-17666.

[32] K. Sasaki, J.X. Wang, H. Naohara, N. Marinkovic, K. More, H. Inada, R.R. Adzic, Recent advances in platinum monolayer electrocatalysts for oxygen reduction reaction: Scale-up synthesis, structure and activity of Pt shells on Pd cores, Electrochim. Acta, **2010**, 55, 2645-2652.

[33] A. Sarkar, A. Manthiram, Synthesis of Pt@Cu Core-shell nanoparticles by galvanic displacement of Cu by Pt4+ ions and their application as electrocatalysts for oxygen reduction reaction in fuel cells, J. Phys. Chem. C, **2010**, 114, 4725-4732.

[34] V. Mazumder, M. Chi, K.L. More, S. Sun, Core/Shell Pd/FePt nanoparticles as an active and durable catalyst for the oxygen reduction reaction, J. Am. Chem. Soc., **2010**, 132, 7848-7849.

[35] K.D. Beard, D. Borrelli, A.M. Cramer, D. Blom, J.W. Van Zee, J.R.

Monnier, Preparation and structural analysis of carbon-supported co core/pt shell electrocatalysts using electroless deposition methods, ACS Nano, **2009**, 3, 2841-2853.

[36] P. Mani, R. Srivastava, P. Strasser, Dealloyed Pt-Cu core-shell nanoparticle electrocatalysts for use in PEM fuel cell cathodes, J. Phys. Chem. C, **2008**, 112, 2770-2778.

[37] S. Koh, P. Strasser, Electrocatalysis on bimetallic surfaces: Modifying catalytic reactivity for oxygen reduction by voltammetric surface dealloying, J. Am. Chem. Soc., **2007**, 129, 12624-12625.

[38] C. Hsu, C. Huang, Y. Hao, F. Liu, Synthesis of highly active and stable Au-PtCu core-shell nanoparticles for oxygen reduction reaction, PCCP, **2012**, 14, 14696-14701.

[39] Y. Zhang, Q. Huang, Z. Zou, J. Yang, W. Vogel, H. Yang, Enhanced durability of Au cluster decorated Pt nanoparticles for the oxygen reduction reaction, J. Phys. Chem. C, **2010**, 114, 6860-6868.

[40] G.R. Zhang, B.Q. Xu, Surprisingly strong effect of stabilizer on the properties of Au nanoparticles and Pt^Au nanostructures in electrocatalysis, Nanoscale, **2010**, 2, 2798-2804.

[41] H.Y. Park, T.Y. Jeon, J.H. Jang, S.J. Yoo, K.H. Choi, N. Jung, Y.H. Chung, M. Ahn, Y.H. Cho, K.S. Lee, Y.E. Sung, Enhancement of oxygen reduction reaction on PtAu nanoparticles via CO induced surface Pt enrichment, Applied Catalysis B: Environmental, **2013**, 129, 375-381.

[42] T.H. Yeh, C.W. Liu, H.S. Chen, K.W. Wang, Preparation of carbon-

supported PtM (M = Au, Pd, or Cu) nanorods and their application in oxygen reduction reaction, Electrochem. Commun., **2013**, 31, 125-128.

[43] K.S. Lee, H.Y. Park, H.C. Ham, S.J. Yoo, H.J. Kim, E. Cho, A. Manthiram, J.H. Jang, Reversible surface segregation of Pt in a Pt3Au/C catalyst and its effect on the oxygen reduction reaction, J. Phys. Chem. C, **2013**, 117, 9164-9170.

[44] D.F. Yancey, L. Zhang, R.M. Crooks, G. Henkelman, Au@Pt dendrimer encapsulated nanoparticles as model electrocatalysts for comparison of experiment and theory, Chemical Science, **2012**, 3, 1033-1040.

[45] R. Lin, H. Zhang, T. Zhao, C. Cao, D. Yang, J. Ma, Investigation of Au@Pt/C electro-catalysts for oxygen reduction reaction, Electrochim. Acta, **2012**, 62, 263-268.

[46] L. Kuai, B. Geng, S. Wang, Y. Sang, A general and high-yield galvanic displacement approach to Au-M (M=Au, Pd, and Pt) core-shell nanostructures with porous shells and enhanced electrocatalytic performances, Chemistry - A European Journal, **2012**, 18, 9423-9429.

[47] S.M. Jeong, M.K. Kim, G.P. Kim, T.Y. Kim, S.H. Baeck, Preparation of Pt-Au/carbon catalysts by a reduction method and their electrocatalytic activities for oxygen reduction reactions, Chem. Eng. J., **2012**, 198-199, 435-439.

[48] Y. Iijima, Y. Takahashi, K.I. Matsumoto, T. Hayashi, N. Todoroki, T. Wadayama, Oxygen reduction reaction activities of Pt/Au(1 1 1) surfaces prepared by molecular beam epitaxy, J. Electroanal. Chem., **2012**, 685, 79-85.

[49] H. Inoue, K. Hayashi, M. Chiku, E. Higuchi, Electrocatalytic activity for oxygen reduction reaction of Au core/Pt shell catalysts, in, vol. 41, 2011, pp. 2237-2243.

[50] Y.H. Fang, Z.P. Liu, Mechanism of oxygen electro-reduction on Au-modified Pt: Minimizing O coverage and pt site exposure toward highly stable and active cathode, J. Phys. Chem. C, **2011**, 115, 17508-17515.

[51] N. Cheng, H. Li, G. Li, H. Lv, S. Mu, X. Sun, M. Pan, Highly active Pt@Au nanoparticles encapsulated in perfluorosulfonic acid for the reduction of oxygen, Chem. Commun., **2011**, 47, 12792-12794.

[52] Y. Ma, H. Zhang, H. Zhong, T. Xu, H. Jin, X. Geng, High active PtAu/C catalyst with core-shell structure for oxygen reduction reaction, Catal. Commun., **2010**, 11, 434-437.

[53] B. Brown, S.D. Wolter, B.R. Stoner, J.T. Glass, Alloying effects of cosputtered gold-platinum thin films on the oxygen reduction reaction in acidic electrolyte, J. Electrochem. Soc., **2008**, 155, B852-B859.

[54] K.S. Lee, I.S. Park, H.Y. Park, T.Y. Jeon, Y.E. Sung, PtRu overlayers on Au nanoparticles for methanol electro-oxidation, Catal. Today, **2009**, 146, 20-24.

[55] I.S. Park, K.S. Lee, Y.H. Cho, H.Y. Park, Y.E. Sung, Methanol electro-oxidation on carbon-supported and Pt-modified Au nanoparticles, Catal. Today, **2008**, 132, 127-131.

[56] I.S. Park, K.S. Lee, J.H. Choi, H.Y. Park, Y.E. Sung, Surface structure

of Pt-modified Au nanoparticles and electrocatalytic activity in formic acid electro-oxidation, J. Phys. Chem. C, **2007**, 111, 19126-19133.

[57] T.Y. Jeon, N. Pinna, S.J. Yoo, D. Ahn, S.H. Choi, M.G. Willinger, Y.H. Cho, K.S. Lee, H.Y. Park, S.H. Yu, Y.E. Sung, Selective deposition of Pt onto supported metal clusters for fuel cell electrocatalysts, Nanoscale, **2012**, 4, 6461-6469.

[58] T.Y. Jeon, N. Pinna, S.J. Yoo, S.H. Yu, S.K. Kim, S. Lim, D. Peck, D.H. Jung, Y.E. Sung, Enhanced activity of Pt-based electrocatalysts for oxygen reduction via a selective Pt deposition process, J. Electroanal. Chem., **2011**, 662, 70-79.

[59] F.R. Fan, D.Y. Liu, Y.F. Wu, S. Duan, Z.X. Xie, Z.Y. Jiang, Z.Q. Tian, Epitaxial growth of heterogeneous metal nanocrystals: From gold nano-octahedra to palladium and silver nanocubes, J. Am. Chem. Soc., **2008**, 130, 6949-6951.

[60] X. Teng, M. Feygenson, Q. Wang, J. He, W. Du, A.I. Frenkel, W. Han, M. Aronson, Electronic and magnetic properties of ultrathin Au/Pt nanowires, Nano Lett., **2009**, 9, 3177-3184.

[61] P.A. Bouit, A. Escande, R. Szücs, D. Szieberth, C. Lescop, L. Nyulászi, M. Hissler, R. Réau, Dibenzophosphapentaphenes: Exploiting P chemistry for gap fine-tuning and coordination-driven assembly of planar polycyclic aromatic hydrocarbons, J. Am. Chem. Soc., **2012**, 134, 6524-6527.

[62] S. Tokonami, N. Morita, K. Takasaki, N. Toshima, Novel synthesis, structure, and oxidation catalysis of Ag/Au bimetallic nanoparticles, J. Phys. Chem. C, **2010**, 114, 10336-10341.

[63] E. Bus, J.A. Van Bokhoven, Electronic and geometric structures of supported platinum, gold, and platinum-gold catalysts, J. Phys. Chem. C, **2007**, 111, 9761-9768.

[64] A. Sarkar, J.B. Kerr, E.J. Cairns, Electrochemical oxygen reduction behavior of selectively deposited platinum atoms on gold nanoparticles, ChemPhysChem, **2013**, 14, 2132-2142.

[65] D.F. Van Der Vliet, C. Wang, D. Li, A.P. Paulikas, J. Greeley, R.B. Rankin, D. Strmcnik, D. Tripkovic, N.M. Markovic, V.R. Stamenkovic, Unique electrochemical adsorption properties of Pt-skin surfaces, Angew. Chem. Int. Ed., **2012**, 51, 3139-3142.

[66] M. Arenz, K.J.J. Mayrhofer, V. Stamenkovic, B.B. Blizanac, T. Tomoyuki, P.N. Ross, N.M. Markovic, The effect of the particle size on the kinetics of CO electrooxidation on high surface area Pt catalysts, J. Am. Chem. Soc., **2005**, 127, 6819-6829.

[67] K.J.J. Mayrhofer, M. Arenz, B.B. Blizanac, V. Stamenkovic, P.N. Ross, N.M. Markovic, CO surface electrochemistry on Pt-nanoparticles: A selective review, Electrochim. Acta, **2005**, 50, 5144-5154.

[68] P. Urchaga, S. Baranton, C. Coutanceau, G. Jerkiewicz, Evidence of an Eley-Rideal mechanism in the stripping of a saturation layer of chemisorbed CO on platinum nanoparticles, Langmuir, **2012**, 28, 13094-13104.

[69] G.R. Zhang, D. Zhao, Y.Y. Feng, B. Zhang, D.S. Su, G. Liu, B.Q. Xu, Catalytic Pt-on-Au nanostructures: Why Pt becomes more active on smaller Au particles, ACS Nano, **2012**, 6, 2226-2236.

[70] B. Hammer, O.H. Nielsen, J.K. Nørskov, Structure sensitivity in adsorption: CO interaction with stepped and reconstructed Pt surfaces, Catal. Lett., **1997**, 46, 31-35.

[71] B. Hammer, J.K. Nørskov, Theoretical surface science and catalysis-calculations and concepts, in, vol. 45, 2000, pp. 71-129.

[72] T. Jiang, D.J. Mowbray, S. Dobrin, H. Falsig, B. Hvolbœk, T. Bligaard, J.K. Nørskov, Trends in CO oxidation rates for metal nanoparticles and close-packed, stepped, and kinked surfaces, J. Phys. Chem. C, **2009**, 113, 10548-10553.

[73] M. Eyrich, T. Diemant, H. Hartmann, J. Bansmann, R.J. Behm, Interaction of CO with structurally well-defined monolayer PtAu/Pt(111) surface alloys, J. Phys. Chem. C, **2012**, 116, 11154-11165.

[74] S. Yang, H. Lee, Atomically dispersed platinum on gold nano-octahedra with high catalytic activity on formic acid oxidation, ACS Catalysis, **2013**, 3, 437-443.

[75] J. Suntivich, Z. Xu, C.E. Carlton, J. Kim, B. Han, S.W. Lee, N. Bonnet, N. Marzari, L.F. Allard, H.A. Gasteiger, K. Hamad-Schifferli, Y. Shao-Horn, Surface composition tuning of Au-Pt bimetallic nanoparticles for enhanced carbon monoxide and methanol electro-oxidation, J. Am. Chem. Soc., **2013**, 135, 7985-7991.

[76] H. Xin, A. Holewinski, S. Linic, Predictive structurereactivity models for rapid screening of pt-based multimetallic electrocatalysts for the oxygen reduction reaction, ACS Catalysis, **2012**, 2, 12-16.

[77] B. Hammer, Y. Morikawa, J.K. Nørskov, CO chemisorption at metal surfaces and overlayers, Phys. Rev. Lett., **1996**, 76, 2141-2144.

[78] R. Hoffmann, A chemical and theoretical way to look at bonding on surfaces, Reviews of Modern Physics, **1988**, 60, 601-628.

[79] B. Hammer, J.K. Norskov, Why gold is the noblest of all the metals, Nature, **1995**, 376, 238-240.

[80] X. Teng, W. Han, Q. Wang, L. Li, A.I. Frenkel, J.C. Yang, Hybrid Pt/Au nanowires: Synthesis and electronic structure, J. Phys. Chem. C, **2008**, 112, 14696-14701.

[81] R.E. Rettew, S. Cheng, M. Sauerbrey, T.A. Manz, D.S. Sholl, C. Jaye, D.A. Fischer, F.M. Alamgir, Near surface phase transition of solute derived Pt monolayers, Top. Catal., **2013**, 56, 1065-1073.

[82] S.E. Hörnström, L. Johansson, A. Flodström, R. Nyholm, J. Schmidt-May, Surface and bulk core level binding energy shifts in PtAu alloys, Surf. Sci., **1985**, 160, 561-570.

[83] J.A. Rodriguez, D.W. Goodman, The nature of the metal-metal bond in bimetallic surfaces, Science, **1992**, 257, 897-903.

[84] A.S. Bandarenka, A.S. Varela, M. Karamad, F. Calle-Vallejo, L. Bech, F.J. Perez-Alonso, J. Rossmeisl, I.E.L. Stephens, I. Chorkendorff, Design of an active site towards optimal electrocatalysis: Overlayers, surface alloys and near-surface alloys of Cu/Pt(111), Angew. Chem. Int. Ed., **2012**, 51, 11845-11848.

[85] L. Pauling, Atomic radii and interatomic distances in metals, J. Am. Chem. Soc., **1947**, 69, 542-553.

[86] R. Smoluchowski, Anisotropy of the electronic work function of metals, Physical Review, **1941**, 60, 661-674.

[87] W.J. Huang, R. Sun, J. Tao, L.D. Menard, R.G. Nuzzo, J.M. Zuo, Coordination-dependent surface atomic contraction in nanocrystals revealed by coherent diffraction, Nat. Mater., **2008**, 7, 308-313.

[88] Y.H. Lee, G. Kim, M. Joe, J.H. Jang, J. Kim, K.R. Lee, Y.U. Kwon, Enhancement of electrocatalytic activity of gold nanoparticles by sonochemical treatment, Chem. Commun., **2010**, 46, 5656-5658.

[89] J. Kim, J.H. Jang, Y.H. Lee, Y.U. Kwon, Enhancement of electrocatalytic activity of platinum for hydrogen oxidation reaction by sonochemically synthesized WC1-x nanoparticles, J. Power Sources, **2009**, 193, 441-446.

[90] K.S. Suslick, S.B. Choe, A.A. Cichowlas, M.W. Grinstaff, Sonochemical synthesis of amorphous iron, Nature, **1991**, 353, 414-416.

[91] J.T. Miller, A.J. Kropf, Y. Zha, J.R. Regalbuto, L. Delannoy, C. Louis, E. Bus, J.A. van Bokhoven, The effect of gold particle size on Au{single bond}Au bond length and reactivity toward oxygen in supported catalysts, J. Catal., **2006**, 240, 222-234.

[92] A. Balerna, E. Bernieri, P. Picozzi, A. Reale, S. Santucci, E. Burattini, S. Mobilio, A structural investigation on small gold clusters by EXAFS, Surf.

Sci., **1985**, 156, 206-213.

[93] P.P. Fang, S. Duan, X.D. Lin, J.R. Anema, J.F. Li, O. Buriez, Y. Ding, F.R. Fan, D.Y. Wu, B. Ren, Z.L. Wang, C. Amatore, Z.Q. Tian, Tailoring Au-core Pd-shell Pt-cluster nanoparticles for enhanced electrocatalytic activity, Chemical Science, **2011**, 2, 531-539.

국문초록

백금 / 금 나노입자의 전자구조 및 기하학적 구조연구와 그에 따른 전기화학적 활성연구

수소연료전지는 높은 효율과 친환경적인 발전과정의 장점으로 화석연료를 대체할 수 있는 신 재생 에너지로 각광받고 있다. 연료극에서의 수소산화 반응에 비해 매우 느린 공기극의 산소환원반응의 활성을 높이기 위한 연구가 수년 간 활발히 진행되었다. 계산과학을 기반으로 한 다양한 분석을 바탕으로 높은 활성이 기대되는 물질들의 연구가 집중 되었다. 단일 금속중에 가장 활성이 높은 백금의 전자구조 분석을 통해, 활성 향상을 위해서는 산소환원반응의 연료 및 중간 생성물인 산소 흡착종간의 세기가 약 0.2 eV 약해져야 한다는 계산 결과를 통해 백금 대비 흡착종과의 결합세기를 줄이기 위한 노력이 진행 되었다. 그 중에서 백금 / 금 구조는 코어의 금이 쉘인 백금에 기하학적으로 인장 변형이 가해져, 백금 원자들간의 오비탈 혼성도의 감소로 인한 d- band 구조의 변화로 흡

착종과의 결합력이 증가할 것으로 예측 되었다. 따라서 산소환원반응 촉매로서의 불리한 점으로 인해 많은 연구가 진행되지 못했다.

이 연구에서는 기존의 계산 결과 및 기존의 단결정 실험결과에서 벗어나 나노 크기의 백금 / 금 촉매의 산소 환원 반응 적용 및 가능성을 검토해 보았다. 코어(금)-쉘(백금) 구조의 나노 촉매를 2단계 과정을 거쳐 합성하였고 또한 금-백금 합금 나노 촉매를 합성하여 분석하였다. 나노 촉매의 구조를 정확히 분석하기 위해 투과전자현미경, x-선 회절 분석기를 이용하였다. 또한 좀 더 정밀한 분석을 위해 가속기를 기반으로 한 x-선 광전자 분석기, x-선 흡수 미세구조분석법을 적용하여 나노 입자의 원자간의 결합길이, 배위수 그리고 전자구조에 대한 분석을 진행하였다. 백금 / 금 나노입자의 표면 백금량에 따른 일산화탄소 전기적 산화 실험결과를 보면, 특정 백금표면 비율까지는 백금과 일산화탄소의 흡착세기가 순수 백금에 비해 증가한 것을 확인 할 수 있었다. 하지만 일정 비율이상의 백금이 표면에 노출 된 경우 백금과 일산화탄소의 흡착세기가 순수 백금에 비해 감소한 것을 확인 할 수 있었다. 이는 기존 계산결과에서 유추할 수 있는 인장 변형효과에 따른 d-band 변화양상과 반대되는 경향임을 확인했다. 실험 결과를 뒷받침 하기 위해 양자역학을 기반으로 한 해석을 시도 하였다. 백금과 일산화탄소 또는 산소종 과의 흡착세기 변화는 d-band 특성의 대표값인

d-band 중심값과 그리고 오비탈 반발력 항목으로 나눠서 생각할 수 있었다. 앞의 d-band 중심 값은 기존의 이론에 따른 변형율에 따른 원자들간의 오비탈 혼성화도 변화와 그에 따른 d- band 두께의 변화와 연관되는 항목으로 흡착종과의 강한 인력을 설명할 수 있다. 오비탈 반발력 항목은 백금 원소주변의 전기음성도 변화에 따른 전자구조 변화에 비례하는 값으로 기존의 산소환원반응 촉매 스크린에서 제외되었던 항목이었다. 그 이유는 대부분의 d 금속들의 전기 음성도가 백금과 유사하기 때문에 큰 무리가 없었기 때문이다. 하지만 금의 경우 백금과의 큰 전기 음성도 차이로 인해 이 항목을 무시 하기 어렵다. 백금과 금의 전기음성도 차이에 의한 백금에서 금으로의 전자 이동과 그에 따른 흡착종과 백금간의 거리가 가까워질 것으로 예측되었다. 흡착종과의 거리 감소로 인한 백금 오비탈과의 반발력의 증대로 인해 백금과의 흡착세기가 약해질 것으로 예측 되었다. 이 2개의 항목이 백금의 표면 비율에 따라 조절됨을 확인 하였다. 백금의 표면비율이 적은 코어-쉘의 경우 변형률의 영향이 큰 이유로, 오비탈 반발력이 주효하지 못한 반면, 표면 백금양의 증가에 따른 변형률의 감소로 특정 비율이상에서는 오비탈 반발력 항목이 주효해 흡착종과의 세기가 약해진 것으로 설명 할 수 있었다. 백금에서 금으로의 전자이동은 x-선 흡수 분광법과 x-선 광전자 여기법으로 확인하였다. 하지만 합금의

경우 전기음성도 차이에 따른 백금에서 금으로의 전자 이동이 아닌 금에서 백금으로의 전자이동이 확인 되었고 이에 따라 코어-쉘에 비해 불리한 구조라는 것을 확인 할 수 있었다. 산소환원반응 실험결과, 일산화탄소 전기산화반응의 경향성과 일치하는 것을 확인 할 수 있었다.

나노 입자의 결과와 기존 단결정 실험에서의 차이점의 원인을 나노 입자의 표면 원자의 배위수에 따른 원자간 거리의 감소를 바탕으로 나노 입자의 표면 원자간의 거리 수축으로 예상 하였다. 원자간 거리 감소로 인한 변형률의 감소로 흡착세기 증가 항목이 제한 될 것으로 예측할 수 있었다. 이를 좀 확인하기 위하여 동일한 크기의 나노 입자에서 표면 배위수를 조절하는 방법을 적용하였다. 초음파 화학적 방법을 적용하여 금 나노 입자의 표면 배위수를 조절하였다. 이를 확인하기 위해 x-선 미세구조 흡수광역분석법을 적용하였다. 배위수의 변화 및 그에 따른 원자간 결합거리의 감소 그리고 복잡도가 증가한 것을 확인하였다. 또한 전기화학적 방법으로 수소 산화 반응을 측정한 결과 표면 배위수가 줄어있는 금 나노 입자에서의 활성이 표면 배위수가 큰 금 나노 입자에 비해 월등히 증가했음을 확인했다. 표면 배위구조가 조절된 금 나노입자 위에 백금을 올린 후에 x-선 미세 회절 구조분석결과, 백금의 격자거리가 줄어있음을 확인하였다. 이는 낮은 배위원자에 의한 수축

효과로 볼 수 있었다. 배위수 조절된 금 나노 입자 위에 올린 백금 나노 입자의 산소환원반응 그리고 일산화탄소 전기산화반응 결과, 배위수가 줄어있는 금위에 백금을 올린 나노 입자의 경우 흡착종과의 감소를 확인하였다. 양자역학을 기반으로 한 흡착종과의 세기를 결정 짓는 요소를 고찰하고 이 효과가 코어 (금)위에 올린 쉘(백금)에 따라 조절 됨을 확인하였다. 이를 바탕으로 나노 입자의 표면 배위수에 따른 원자간 거리 조절효과를 적용하여 높은 산소환원반응 활성뿐만 아니라 장기안정성에서도 우수한 나노 촉매를 제안하였다. 나노 촉매 디자인의 기초연구를 통하여 흡착 종과의 세기 변화 원인을 분석 및 적용을 통하여 새로운 나노 입자 촉매 디자인에 활용될 것으로 기대 된다.

주요어: 전기화학, 전자 및 기하학적 구조, 나노입자, 산소환원반응, 백금/금.

학번:2010-22821

감사의 글

감사의 글을 적으려고 자리에 앉으니 문득 대학원에 처음 들어왔던 날이 기억납니다. 어색함은 물론이고 유난히도 시간이 흐르지 않는 것만 같은 느낌이 들었습니다. 랩미팅에 들어가면 알아 들을 수 없는 내용에 걱정과 두려움이 많았습니다. 시간이 지나 졸업하는 선배들의 논문심사 발표를 보면서 부러움과 동시에 언젠가 설 제 모습을 상상 했었습니다. 이제 제 차례가 되어 떠날 때가 되었다고 생각하니 기분이 좋으면서도 섭섭한 마음이 듭니다.

부족한 저를 믿어주시고 항상 지지해주신 성영은 교수님께 감사 드립니다. 연구뿐만 아니라 인생을 살아가는 데 있어 조언해주신 교수님의 말씀을 항상 간직하며 살겠습니다. 연구자가 지녀야 할 자세와 연구 방향에 대해서 진심으로 조언해 주신 현택환 교수님께 감사 드립니다. 학부 때 처음 뵙고 제가 연구자의 길로 진로를 정할 수 있게 롤 모델이 되어주신 이현주 교수님께 감사합니다. 바쁘신 와중에 학위심사 위원으로 지도해주시고 조언해 주신 최원용, 김도희 교수님께도 진심으로 감사합니다. 부족함이 많은 제게 조언해 주신 많은 사항을 통해 발전 할 수 있도록 노력하겠습니다.

또한 멀리서 항상 신경 써주시고 도와주신 유성종 박사님, 어려움이 있을 때마다 도움을 청했던 문봉진 교수님께도 진심으로 감사 인사 드립니다. 항상 힘들었을 때 옆에 있어 줬던 많은 연구실 선,후배 그리고 친구들에게도 감사의 인사를 전합니다. 어느 술자리에서 박사학위를 받는 다는

것의 의미에 대해 이야기를 나눴던 일이 기억납니다. 그 당시 제 대답은 매사에 최선을 다할 뿐 의미를 잘 모르겠다고 답했던 것 같습니다. 사실 아직도 의미를 잘 몰라 부끄러운 마음이 듭니다. 다만 학위를 받는 것이 끝이 아닌 새로운 시작임을 기억하며 연구실에 처음 왔던 마음 가짐으로 항상 최선을 다하는 삶을 살 수 있도록 노력하겠습니다. 인생을 살아감에 있어서 학위과정에서의 추억이 항상 힘이 되길 바라며, 제 자신에게 부끄럽지 않은 사람이 되겠습니다.

마지막으로 항상 저를 믿고 배려해주신 부모님과 챙겨준 누나에게 감사합니다. 항상 응원해주시고 지켜봐 주셨던 모든 분들께 감사합니다.

2014년 1월 21일

정 동 영 올림